Astron. & Astrophys. 47, 263—292 (1976)

Dynamical Evolution of the Triple System of the Galaxy, the Large and Small Magellanic Clouds

Mitsuaki Fujimoto and Yoshiaki Sofue
Department of Physics, Nagoya University, Chikusa, Nagoya

Received January 3, revised September 9, 1975

Summary. Obtained here are some series of orbits of the Large and Small Magellanic Clouds (LMC and SMC) round the Galaxy, along which the two Clouds were in a binary state for the last 5 to 10×10^9 years. Approximately nine hundred test particles are distributed in the Galaxy, the LMC and SMC so as to simulate their continuous media. The dynamical behavior of these particles is followed numerically and compared with the bending of the galactic disk and with the "Magellanic Stream". This enables us to choose some probable orbits of the LMC: The peri- and apogalactic distances of the LMC's orbit seem to be about 30 kpc and 60–80 kpc, respectively. The tilt angle of the orbital plane to the galactic disk is 70° to 110° with the ascending and descending nodes respectively at $l \approx 280°$ and 55°. The perigalacticon is approximately in the direction of $(l, b) = (65°, -40°)$. Some constraints are also given to the motion of the SMC: Its present velocity relative to the LMC cannot be more than 70 km/s, and the separation of the LMC and SMC seems to have oscillated between 10 kpc and 40 kpc for the last 5×10^9 years.
Also discussed in relation to the dynamics of the triple system of the Galaxy, LMC and SMC are the velocity dispersion of common stars, high-velocity H I clouds, high-velocity A-type stars in the Galaxy, distant gaseous spiral arms at 20 to 30 kpc from the galactic center, and north-south asymmetry of our rotation curves.

Key words: the Galaxy – Magellanic Clouds – multiple system – tidal interaction – bending

I. Introduction

It has been known since about 1957 that the hydrogen gas layer in our Galaxy is warped upward by several hundred parsecs at the northern sector of its outer part and downward at the opposite side, namely that facing the Magellanic Clouds [see, e.g., Kerr and Westerhout (1965) for the bending structure]. According to recent extensive surveys of the neutral hydrogen gas, the displacement of the gas layer from the equatorial plane has seemed to amount to as much as 1–6 kpc at galactocentric distances $R = 15$–25 kpc and at longitudes of $l = 50°$ to 150° (Henderson, 1966; Kepner, 1970; Davies, 1972; Verschuur, 1973).
Various orbits of the Large Magellanic Cloud (LMC) round the Galaxy have been considered for explaining the bending of the galactic disk in terms of a tidal force due to the LMC. Elwert and Hablick (1965) and Avner and King (1967) assumed approximately circular orbits a priori for the revolution of the LMC round the galactic center and evaluated the perturbing force on stars in the Galaxy. They claimed that if the radius of the orbit is 50 kpc and the mass of the LMC is $10^{10}\, M_\odot$, the tidal force causes a secular increase in distortion of the galactic plane, eventually tending to the observed bending. Hunter and Toomre (1969) and Toomre (1972) thought those estimates to have been much too optimistic; they advocated instead a close passage of the LMC within a distance of 20 kpc of the galactic center about 5×10^8 years ago, from their mathematical study of infinitesimal bending oscillations and responses of a self-gravitating disk.
Hydrogen gas around and trailing from the Magellanic Clouds forms a narrow band on the sky, the "Magellanic Stream" (Mathewson *et al.*, 1974) on which some high-velocity H I clouds are also located. This band is nearly along a great circle which passes by the galactic poles and crosses over the galactic equator at $l = 100°$ and 280°. Guessing that the hydrogen stream is gaseous "debris" left behind from the condensation of the two galaxies, Mathewson *et al.* thought that the orbital plane of the Magellanic Clouds is nearly perpendicular to the galactic plane, and that the pericenter distance of the orbit is at least 40 kpc.
The above variety of orbits of the LMC seems due to the fact that the points stressed by different authors were not the same and the observational data which they took into account was not uniform. One of the aims of the present paper is to try and determine more probable orbits of the LMC and SMC (Small Magellanic Cloud) by postulating that the two have been in a binary state for the last 5–10×10^9 years and that both the bending

of the galactic disk and the "Magellanic Stream" were produced by the gravitational interaction among the Galaxy, LMC and SMC. The former postulate seems to be sound in view of the common diffuse H I gas around the LMC and SMC (Hindman *et al.*, 1963) and of the polarization planes of bright stars and H II regions which are predominantly parallel to the line joining them (Mathewson and Ford, 1970; Schmidt, 1971).

The tidal influence of the Galaxy on the Magellanic Clouds has also attracted a few authors already. Among them de Vaucouleurs (1960) judged from his deeply-exposed photograph that a faint envelope extends from the LMC toward the Galaxy; he blamed our tidal force acting upon the LMC. More recently, Clutton-Brock (1972), Mirabel and Turner (1973), Toomre (cited in Mirabel and Turner) made theoretical and observational studies of tidal disruption effect among the Magellanic Clouds.

It is obviously another aim of this paper to study also such dynamical phenomena of the interstellar medium as a whole in the gravitationally interacting triple system of the Galaxy, the LMC and SMC.

II. Approximate Orbits of the LMC for the Last Several Billions of Years

The masses of the LMC and SMC have been observationally estimated as $5\text{–}20\times10^9\ M_\odot$ and $1\text{–}2\times10^9\ M_\odot$, respectively (Hindman *et al.*, 1963; Hindman, 1967; de Vaucouleurs, 1960). Throughout the present paper we adopt $2\times10^{10}\ M_\odot$ for the mass of the LMC and $2\times10^9\ M_\odot$ for the SMC. As the mass of the Galaxy, we take $1.2\times10^{11}\ M_\odot$ from Innanen's model 10-252 (1966). Since the mass of the LMC is much greater than that of the SMC, the LMC can be treated as a single object for the first one or two revolutions round the Galaxy. Furthermore if the LMC does not closely approach the galactic center, the gravitational potential due to the Galaxy can be approximated by a point mass potential; we will in fact assume so in computing the orbit of the LMC.

We adopt an inertial reference system whose origin coincides with the center of mass of the Galaxy and

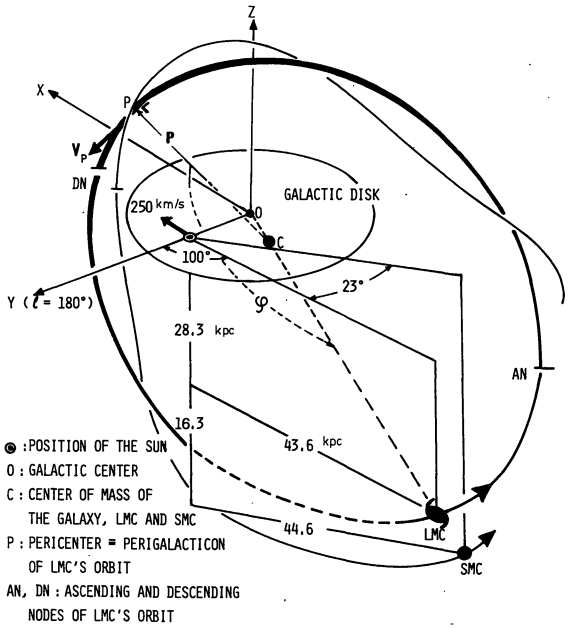

Fig. 1. Schematic bird's eye view of the geometrical relationship of the Galaxy, LMC, and SMC. The origin of the center-of-mass system is at C and its x, y, z axes are parallel to the X, Y, Z axes. Positions of the LMC and SMC at present ($t=0$) are indicated

Table 1

t:	The time reckoned from the present epoch ($t=0$ at present and $t>0$ for future).
$\boldsymbol{r}(x, y, z)$:	The position vector.
$\boldsymbol{r}_G, \boldsymbol{r}_L, \boldsymbol{r}_S$:	The position vectors of the Galaxy, LMC and SMC; $\lvert\boldsymbol{r}_G\rvert=r_G$, $\lvert\boldsymbol{r}_L\rvert=r_L$ and $\lvert\boldsymbol{r}_S\rvert=r_S$.
m_G, m_L, m_S:	The masses of the Galaxy, LMC and SMC which are independent of the coordinate we choose.
$\boldsymbol{p}$:	The position vector of the LMC at the perigalactic instant or at the closest approach to the Galaxy (equivalently to the origin of the coordinates). $\lvert\boldsymbol{p}\rvert=p$.
$\boldsymbol{D}$:	$\boldsymbol{D}=\boldsymbol{p}-\boldsymbol{r}_G$; the position vector of the perigalacticon of the LMC's orbit, referred to the galactic center. $\lvert\boldsymbol{D}\rvert=D$. We have a relation. $D=(1+m_L/m_G)\cdot p$.
v_p:	$\dot{\boldsymbol{r}}_L$ at $\boldsymbol{r}_L=\boldsymbol{p}$; $\lvert\boldsymbol{v}_p\rvert=v_p$.
$\boldsymbol{r}_L^0, \boldsymbol{r}_S^0$:	The position vector of the LMC, and SMC at the present or at $t=0$. $\lvert\boldsymbol{r}_L^0\rvert=r_L^0$ and $\lvert\boldsymbol{r}_S^0\rvert=r_S^0$.
$\boldsymbol{v}_L^0, \boldsymbol{v}_S^0$:	The velocities of the LMC and SMC at $t=0$; their components are $\boldsymbol{v}_L^0=(u_L, v_L, w_L)$ and $\boldsymbol{v}_S^0=(u_S, v_S, w_S)$. It is obvious that $\boldsymbol{v}_L^0=\dot{\boldsymbol{r}}_L^0$ and $\boldsymbol{v}_S^0=\dot{\boldsymbol{r}}_S^0$.
U:	$U^2=u_L^2+v_L^2+w_L^2$.
φ:	The angle between $\boldsymbol{p}$ and $\boldsymbol{r}_L$ measured in the direction of revolution of the LMC.
φ_0:	The angle φ at $\boldsymbol{r}_L=\boldsymbol{r}_L^0$.
$\boldsymbol{e}_{0L}=(\lambda_{0L}, \mu_{0L}, \nu_{0L})$:	The unit vector directed from the origin to the present position of the LMC, that is, $\boldsymbol{r}_L^0/r_L^0$.
$\boldsymbol{e}_{\odot L}=(\lambda_{\odot L}, \mu_{\odot L}, \nu_{\odot L})$:	The unit vector directed from the sun to the present position of the LMC.
$\boldsymbol{e}_{\odot S}=(\lambda_{\odot S}, \mu_{\odot S}, \nu_{\odot S})$:	The unit vector directed from the sun to the present position of the SMC.
$V_{\text{obs. L,S}}$:	The observed radial velocities of the LMC and SMC, corrected for the galactic rotation and the motion of the sun in the Local Standard of Rest (LSR).
$v_{\text{obs. L,S}}$:	Defined as $v_{\text{obs. L,S}}=V_{\text{obs. L,S}}(1+m_L/m_G)$. It is convenient to use these quantities in the center-of-mass coordinates system.
(l, b):	The galactic longitude and latitude.
$\boldsymbol{R}(X, Y, Z)$:	$\boldsymbol{r}-\boldsymbol{r}_G$; the position vector relative to the galactic center. $\lvert\boldsymbol{R}\rvert=R$.

Table 2. Observed kinematical quantities of the LMC and SMC

	LMC	SMC
(l, b)	$(280°, -33°)$	$(303°, -45°)$
v_{obs}; before correction for the galactic rotation and solar motion	260 km/s	150 km/s
V_{obs}	51 km/s	0 km/s
Present positions in the (X, Y, Z) coordinates	$(-43.0, 2.4, -28.3)$ kpc	$(-37.4, -14.3, -44.6)$ kpc
Distance from the Sun	52 kpc	63 kpc
Mass	$m_L = 2\times10^{10}\,M_\odot$	$m_S = 2\times10^{9}\,M_\odot$
Unit vectors	$e_{0L} = (-0.834, 0.047, -0.550)$	
	$e_{\odot L} = (-0.826, -0.146, -0.545)$	$e_{\odot S} = (-0.593, -0.385, -0.707)$

LMC (Fig. 1). The symbols in Table 1 are used throughout the present paper. All the quantities except for $\boldsymbol{R}$, $V_{obs,L}$, $V_{obs,S}$ and (l, b) are defined in this center-of-mass system.

The sun is assumed located in the galactic plane at a galactocentric distance of 10 kpc, at which the velocity of the galactic rotation is 250 km/s. In Table 2 we list the observed kinematical quantities of the LMC and SMC, which will be adopted throughout the present paper.

The equation of motion for the LMC written in these reference coordinate is

$$\frac{d^2\boldsymbol{r}_L}{dt^2} = -\frac{Gm_G}{(1+m_L/m_G)^2}\frac{\boldsymbol{r}_L}{r_L^3}, \tag{1}$$

and of course $\boldsymbol{r}_G = -(m_L/m_G)\boldsymbol{r}_L$. Upon integration we have, on the orbital plane,

$$r_L = \frac{p}{[1-GM/pv_p^2]\cos\varphi + GM/pv_p^2}, \tag{2}$$

where $M = m_G/(1+m_L/m_G)^2$, and $(\boldsymbol{v}_p\times\boldsymbol{p})\cdot\boldsymbol{r}_L = 0$. As usual, the orbit of the LMC is circular for $GM/pv_p^2 = 1$, elliptical for $1 > GM/pv_p^2 \geqq 1/2$, and hyperbolic for $GM/pv_p^2 \leqq 1/2$. When we specify p and v_p, the speed U of the LMC at $\boldsymbol{r}_L = \boldsymbol{r}_L^0$ is evaluated as

$$U^2 = v_p^2 + 2GM(1/r_L^0 - 1/p). \tag{3}$$

The radial component of the LMC velocity $\dot{\boldsymbol{r}}_L$ at $\boldsymbol{r}_L = \boldsymbol{r}_L^0$ is then represented by

$$v_r = U\sin\alpha, \tag{4}$$

with

$$\tan\alpha = (\partial r_L/r_L\partial\varphi)_{r_L=r_L^0}, \tag{5}$$

where φ is defined in Fig. 1 and Table 1.

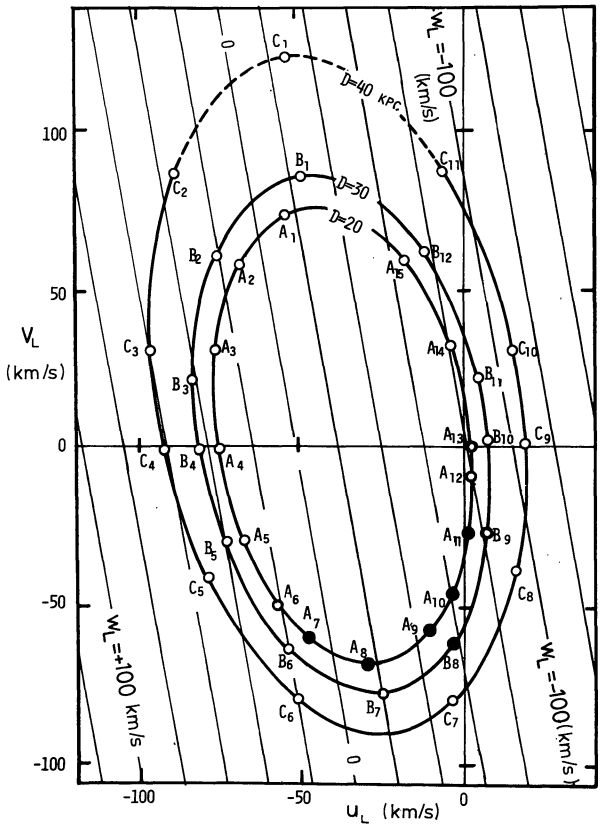

Fig. 2. Present velocity $\boldsymbol{v}_L^0$ of the LMC $(t=0)$, for $D=20$, 30 and 40 kpc. The LMC's orbit on the dashed line is hyperbolic. Our orbit computations refer to $\boldsymbol{v}_L^0$ at the small circles on the ellipses. The LMC velocity at the open circles guarantees a binary state with the SMC for the last 5–10×10^9 years if the SMC's velocity $\boldsymbol{v}_S^0$ is suitably chosen (see Fig. 3). When the SMC remains bound to the Galaxy for more than 5×10^9 years in case $D=20$ kpc, we sometimes meet situations where the binary structure is transiently disrupted. We define in the present paper that the LMC-SMC system is not a binary if $|\boldsymbol{r}_L - \boldsymbol{r}_S| \geqq \{\max(|\boldsymbol{r}_L - \boldsymbol{r}_G|) + \min(|\boldsymbol{r}_L - \boldsymbol{r}_G|)\}/2$ is realized even briefly. With the dark circles of $A_7, A_8 \ldots A_{10}$, this definition often applies

We have

$$(\boldsymbol{e}_{0L}\cdot\boldsymbol{v}_L^0) = \lambda_{0L}u_L + \mu_{0L}v_L + \nu_{0L}w_L = v_r \tag{6}$$

$$(\boldsymbol{e}_{\odot L}\cdot\boldsymbol{v}_L^0) = \lambda_{\odot L}u_L + \mu_{\odot L}v_L + \nu_{\odot L}w_L = v_{obs,L} \tag{7}$$

and

$$(\boldsymbol{v}_L^0\cdot\boldsymbol{v}_L^0) = u_L^2 + v_L^2 + w_L^2 = U^2, \tag{8}$$

where $v_{obs,L}$ is given from the data on radial velocity of the LMC, and v_r and U^2 are evaluated from Eqs. (3), (4) and (5) when p and v_p are specified. As the observed radial velocity of the LMC, we take the value given by Hindman *et al.* (1963), from which we substract contributions due to both the galactic rotation at 250 km/s and also the solar motion at 20 km/s in the direction of $l=56°$, $b=24°$. In terms of symbols from Table 1, the extreme right-hand side of Eq. (7) thus becomes $v_{obs,L} = V_{obs,L}/(1+m_L/m_G) = 44$ km/s, with $V_{obs,L} = 51$ km/s.

Solutions for u_L, v_L and w_L are given graphically in Fig. 2 for the three cases of assumed perigalactic distance

Table 3. Data on the orbits of the LMC and SMC in a binary state for the last $5\sim10\times10^9$ years

	v_L^0 (km/s)			$n=(r_L^0-r_G^0)\times v_L^0/\|(r_L^0-r_G^0)\times v_L^0\|$			i[a]	φ^0	$\|r_L-r_G\|_{max}$[b]	v_S^0 (km/s)[c]					
	(u_L,	v_L,	w_L)	(n_X,	n_Y,	n_Z)			(kpc)	(u_S,		v_S,		w_S)	
$D=20$ kpc															
A_1	−55.1	73.0	−15.2	0.544	0.243	−0.803	37°	126°	87	−57	~ −17	37	~ 62	− 7	~ 23
A_2	−69.1	57.7	10.2	0.446	0.644	−0.621	52	128	82	−60	−27	25	75	−10	35
A_3	−76.3	30.6	28.3	0.254	0.917	−0.307	72	132	75	−50	−30	10	50	10	33
A_4	−75.2	− 0.9	35.1	0.016	0.998	0.060	93	137	68	−50	−27	17	37	18	31
A_5	−67.1	−30.1	30.5	−0.216	0.889	0.403	114	142	63	−40	−20	− 5	15	23	37
										−25	−15	10	14	20	24
A_6	−57.8	−47.5	21.1	−0.360	0.708	0.607	127	145	61	−45	−25	−35	− 5	38	54
										−18	−13	− 5	5	21	24
A_7	−47.0	−59.9	8.0	−0.468	0.467	0.750	139	147	60						
A_8	−36.5	−66.2	6.1	−0.501	0.349	0.792	142	148	59						
A_9	−10.6	−59.1	−47.4	−0.500	−0.485	0.717	136	147	60	no					
A_{10}	− 3.0	−46.4	−62.3	−0.408	−0.723	0.558	124	145	61						
A_{11}	1.8	−28.8	−74.2	−0.276	−0.898	0.342	110	142	63						
A_{12}	2.9	−15.0	−80.0	−0.170	−0.970	0.176	100	140	65	30	35	5	20	−26	−15
A_{13}	2.3	0.7	−83.0	−0.050	−0.999	−0.009	90	137	68	25	35	− 5	5	−15	−10
										20	25	15	20	−15	−12
A_{14}	− 4.7	32.0	−80.7	0.193	−0.908	−0.371	68	132	75	37	43	40	46	−47	−43
A_{15}	−18.8	58.7	−66.4	0.405	−0.625	−0.667	48	128	82	− 7	15	45	65	−35	−22
$D=30$ kpc															
B_1	−50.7	85.9	−25.3	0.552	0.081	−0.830	34	112	76	−50	−15	45	90	− 2	15
B_2	−76.6	59.9	20.9	0.410	0.720	−0.560	56	116	72	−78	−38	17	97	11	54
B_3	−82.7	20.3	40.8	0.160	0.974	−0.160	81	122	66	−65	−30	−10	25	30	60
B_4	−80.9	− 0.6	43.7	0.021	0.998	0.053	93	126	63	−47	−23	7	41	18	30
										−50	−40	−10	0	41	47
										−50	−40	−40	−30	55	65
B_5	−73.2	−30.3	39.9	−0.184	0.916	0.358	111	132	60	−40	−20	− 3	17	22	36
B_6	−53.5	−63.9	19.0	−0.430	0.569	0.701	134	140	57	−25	−10	−20	−10	25	37
B_7	−32.2	−77.3	− 9.7	−0.541	0.121	0.832	146	143	56	−15	0	−45	−35	40	55
										5	15	−35	−30	25	35
										25	35	−50	−45	15	25
B_8	− 3.0	−62.9	−57.8	−0.469	−0.585	0.661	131	140	57	no					
B_9	7.9	−28.7	−83.6	−0.246	−0.924	0.294	107	132	60	55	65	−10	10	−36	−24
B_{10}	7.9	1.2	−91.6	−0.045	−0.999	−0.017	89	126	63	40	55	30	45	−51	−42
										42	52	5	19	−36	−28
B_{11}	4.3	22.0	−91.7	0.095	−0.969	−0.228	77	122	66	22	45	10	52	−35	−25
B_{12}	−11.9	61.2	−77.5	0.363	−0.703	−0.611	52	116	72	10	25	30	50	−31	−24
$D=40$ kpc															
C_4	−91.7	− 1.91	60.4	0.017	0.998	0.058	93	67	148	−110	− 5	−80	70	20	100

[a]) Inclination of $\boldsymbol{n}$ relative to the rotation axis of the Galaxy: $0\leqq i<90°$, direct revolution; $i=90°$, overhead; and $90°<i\leqq180°$, retrograde.
[b]) The apocenter distance in the two-body problem in Section II. In the three-body problem in the potentials (10) and (11) in Section III, however, the maximum distance between the Galaxy and the LMC often exceeds this apocenter distance by ten to twenty percent.
[c]) The capture window in v_S^0 here stems from an eye estimate of the distribution of the open circles in figures like 3a and 3b.

$D=20$, 30 and 40 kpc, where $D=(1+m_L/m_G)p$. Thus, if the present velocity of the LMC is represented by a point on the ellipse of $D=20$ kpc in the figure, for example, both the observed radial velocity of 51 km/s, and the perigalactic distance of 20 kpc are satisfied. For further orbit data see Table 3.

The orbit of the LMC is hyperbolic when the velocity (u_L, v_L, w_L) lies on the dashed part of the $D=40$ kpc ellipse. However, if we assume that the LMC passed or will pass the Galaxy at $D=20$ kpc, its orbit is clearly not hyperbolic but must be elliptical for the parameters used in Table 2.

III. Three-body Problem of the Galaxy, LMC and SMC

For describing the evolution of the actual triple system of the Galaxy, LMC and SMC, the point-mass potential as we have just used is probably not good enough. We therefore assume a slightly oblate potential for the Galaxy,

$$\begin{aligned}\Phi_G &= A/a+B/a^3 \quad \text{for} \quad a\geqq 8\,\text{kpc},\\ &= C\varpi^2+FZ^2 \quad \text{for} \quad a<8\,\text{kpc},\end{aligned} \tag{9}$$

where

$$a=(\sqrt{(\varpi+f)^2+Z^2}+\sqrt{(\varpi-f)^2+z^2})/2$$

with $\varpi^2 = X^2 + Y^2$ (see Fig. 1 for the axes X, Y and Z). The constants A, B and f are chosen so that Φ_G represents the Innanen's (1966) model potential of the Galaxy (model 10-252 in his terms) in the range of $10 \leqq a \leqq 20$ kpc, whereas the constants C and F are selected so that Φ_G and its gradient are continuous at $a = 8$ kpc. Since we are concerned primarily with the motion of the LMC, SMC and test particles at $a > 10$ kpc (in Section IV), the form of the potential (9) for $a < 8$ kpc is not crucial to our discussions. We take $A = 51$, $B = 450$, $C = -0.118$, $F = -0.325$ and $f = 5.2$, in the units of kpc for the length, 100 km/s for the velocity, and therefore about 10^7 years for the time. These parameters correspond to the Galactic mass $m_G = 1.2 \times 10^{11}\ M_\odot$.

For the potentials of the LMC and SMC, we take the Plummer's laws

$$\Phi_{L,S} = Gm_{L,S} / \sqrt{(r - r_{L,S})^2 + K_{L,S}^2}\,, \tag{10}$$

where $K_L = 3$ kpc for the LMC and $K_S = 2$ kpc for the SMC. Equations of motion for the whole system written as follows, in the reference coordinate system with its origin at the center of mass of the three galaxies, are then

$$\ddot{r}_i = \frac{\partial}{\partial r_i} \sum_{i \neq j} \Phi_j(r_i - r_j)\,, \tag{11}$$

where the suffices i and j represent the three galaxies, and Φ_j the gravitational potential due to the j-th galaxy.

To determine the motions of the LMC and SMC in the past ($t < 0$), we integrate Eq. (11) toward the past from the present epoch ($t = 0$) with the initial conditions of the LMC and SMC satisfying the observed positions and radial velocities.

For the LMC we can take a point in Fig. 2 as a reasonable approximation[1]), but for the SMC we have the following condition,

$$\begin{aligned} V_{\mathrm{obs,S}} &= (\dot{r}_S^0 - \dot{r}_G^0) \cdot e_{\odot S} \\ &\simeq v_{\mathrm{obs,S}} + (m_L/m_G)(v_L^0 \cdot e_{\odot S})\,, \end{aligned} \tag{12}$$

where we take into account $m_L \gg m_S$. In turn, since $V_{\mathrm{obs,S}} \approx 0$, we have that

$$\lambda_{\odot S} u_S + \mu_{\odot S} v_S + \nu_{\odot S} w_S \simeq -(v_L^0 \cdot e_{\odot S}) m_L / m_G\,. \tag{13}$$

Thus any velocity $v_S^0(u_S, v_S, w_S)$ that lies on the plane in velocity space described by Eq. (13) is a conceivable initial value for the SMC.

[1]) In the present three-body problem, the pericenter distance of the LMC's orbit has sometimes about ten to twenty percent deviation from that in Section II.

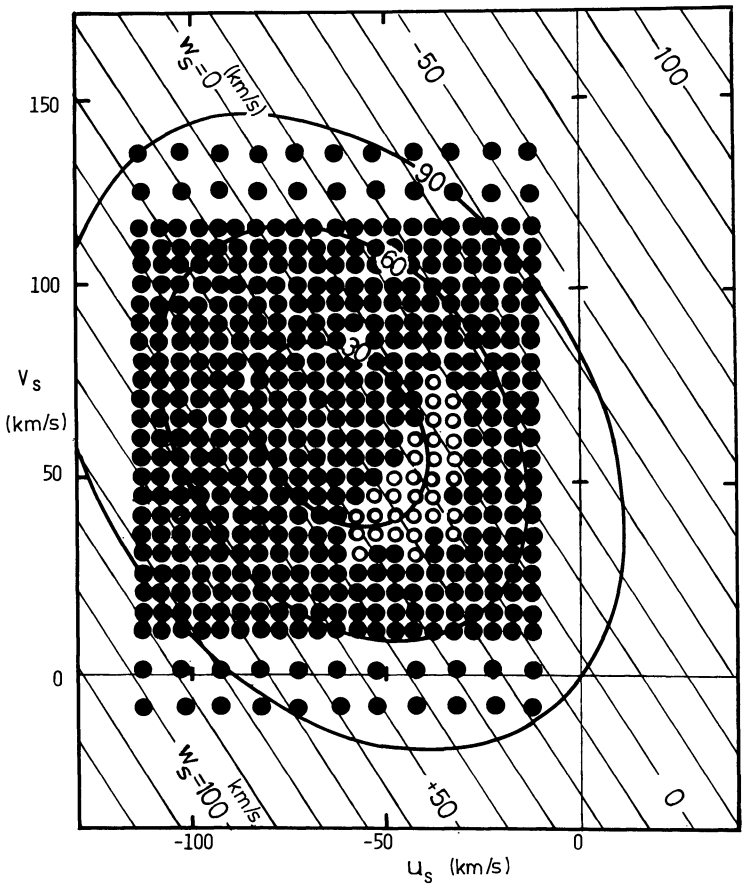

Fig. 3a. Orbit computations of the SMC made for about 500 choices of v_S^0 indicated by the circles, assuming the LMC velocity v_L^0 from point A_2 in Fig. 2. The three ellipses refer to $|v_S^0 - v_L^0| = 30$, 60 and 90 km/s

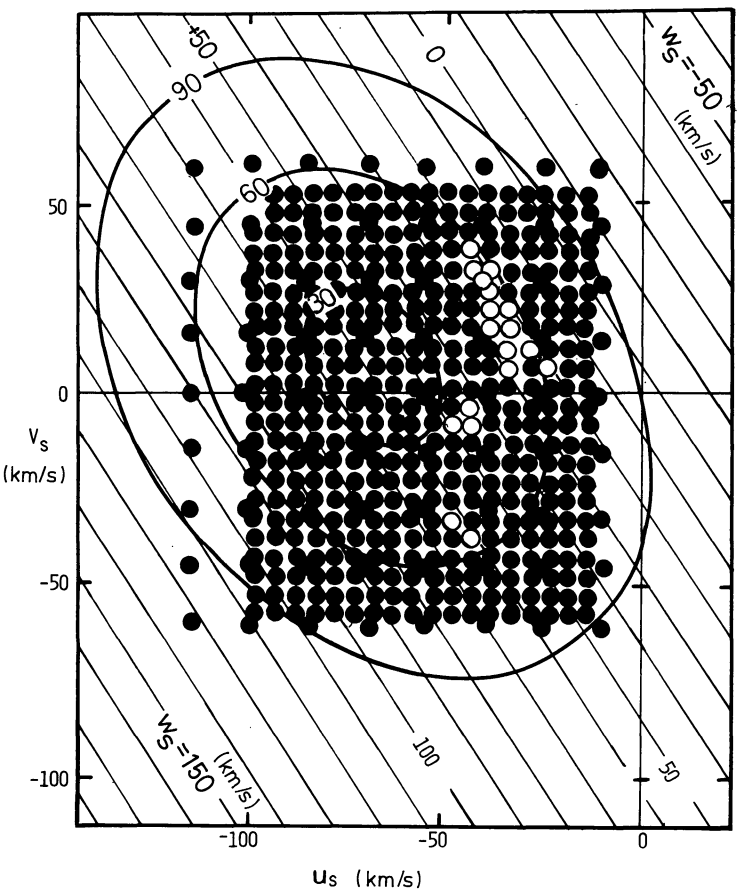

Fig. 3b. Same as Fig. 3a but with the LMC velocity v_L^0 taken to correspond to B_4 in Fig. 2

Two examples of the various orbital outcomes with different choices of v_L^0 and v_S^0, for assumed LMC motions corresponding to points A_2 and B_4 in Fig. 2, are shown in Figs. 3a and b, respectively. From each of these initial values of (u_L, v_L, w_L) and (u_S, v_S, w_S) we integrated Eq. (11) backward some $5–10 \times 10^9$ years. In the large majority of cases, indicated by the filled circles, these calculations revealed that the LMC and SMC would not have been bound to each other in that very distant past. However, we also found that certain specific choices of v_S^0 for these assumed v_L^0 did admit a binary status of the two Clouds over at least 5×10^9 years. Those present velocities have been indicated by the open circles in Figs. 3a and b.

For the choice of v_L implied by Fig. 3a, for instance, these open circles cluster near $u_S = -45$, $v_S = +50$, $w_S = +10$ km/s. More generally, the approximate locations of similar "capture windows" determined by us for various other assumed LMC velocities are listed in Table 3.

The escape velocity of the SMC from the LMC is about 90 km/s for the present separation, $|r_S^0 - r_L^0| = 24$ kpc. As has been noted also by others, the tidal force disrupting the LMC-SMC system at present seems to be larger than the gravitational force binding the two, or

$$(2Gm_G|r_S^0 - r_L^0|/|r_L^0 - r_G^0|^3)/(Gm_L/|r_S^0 - r_L^0|^2) = (2m_G/m_L)|r_S^0 - r_L^0|^3/|r_L^0 - r_G^0|^3 = 1.2 .$$

a) $D = 20$ kpc

In more detail, we first examine the case where the LMC passed the center of the Galaxy at $D = 20$ kpc. Altogether some 4000 of our numerical integrations refer to that case: We considered all fifteen points A_1, $A_2 \ldots A_{15}$ from the $D = 20$ kpc ellipse in Fig. 2 as possible starting velocities v_L^0 of the LMC, and between 200 and 500 SMC velocities v_S^0 for each of those. An example of well-bound orbits so computed (corresponding to about the middle of the capture window in Fig. 3a) is given in Fig. 4a; that integration went back the entire 10^{10} years and showed the LMC and SMC to accompany each other throughout. A less enduring example is illustrated in Fig. 4b: There the Small Cloud disappears from the plot at about $t = -2.7 \times 10^9$ years.

After such extensive computations, we reach the following conclusions. The LMC and SMC could have been in a binary state for the last 5×10^9 years—and often the whole 10^{10} years—, if the LMC's velocity v_L^0 is at the open circles A_{12}, $A_{13} \ldots A_6$ on the $D = 20$ kpc ellipse in Fig. 2, and if the SMC's velocity v_S^0 is chosen to lie in the suitable range in the (u_S, v_S, w_S)-space. Of course the initial velocity v_S^0 of the SMC could in principle have been any point on the plane defined in (u_S, v_S, w_S)-space by Eq. (13), but that capture window (if indeed any) is in fact rather narrow: As indicated in Table 3 and elsewhere, we find that a strict constraint is imposed on the

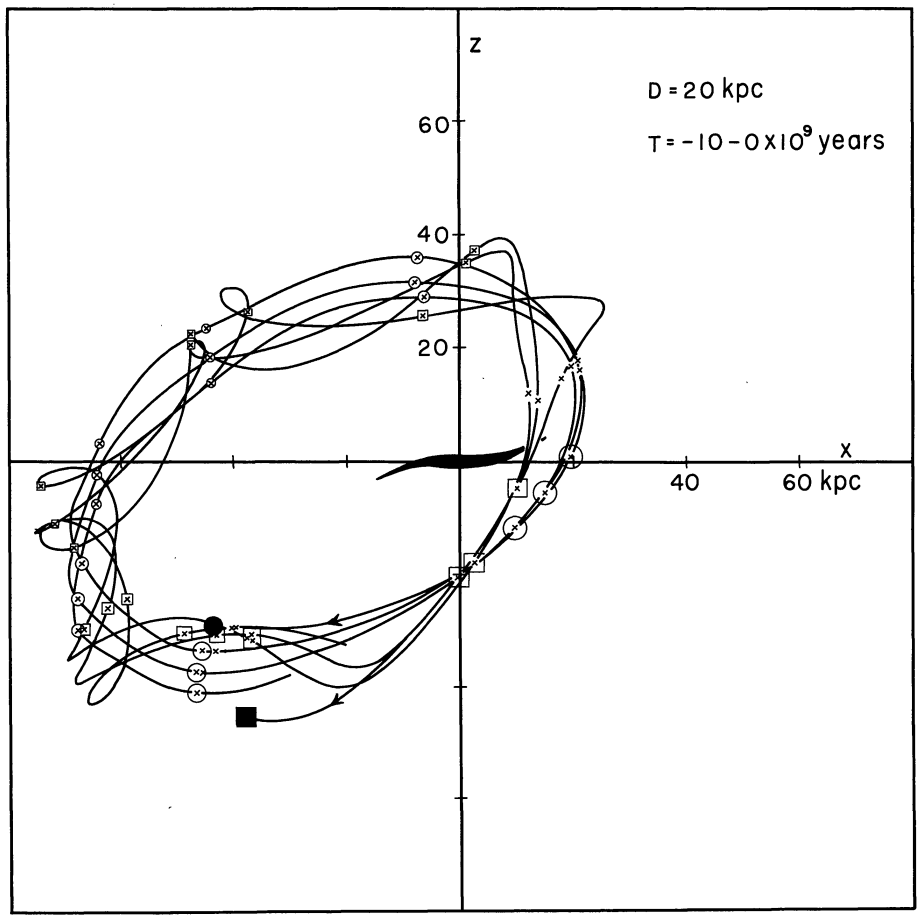

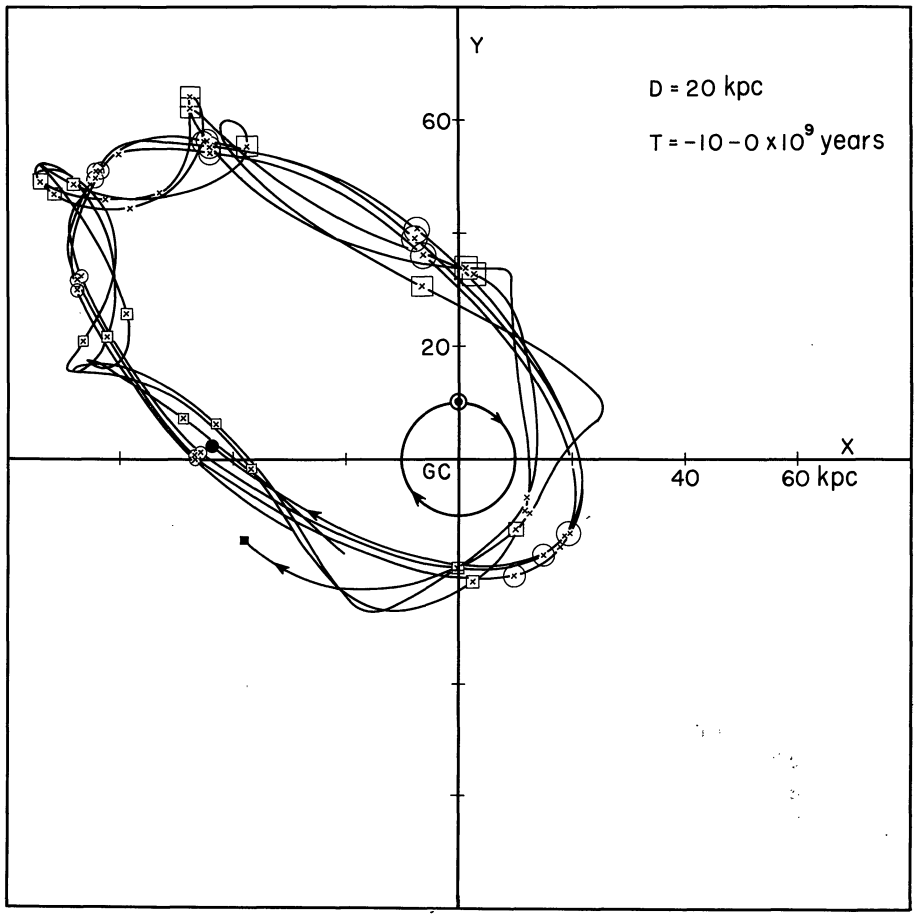

Fig. 4a. Sample $D = 20$ kpc orbits of the LMC and SMC projected onto the (X, Y) and (X, Z) planes, for present velocities $\mathbf{v}_L^0 = (\mathbf{v}_L^0)_{A_2} = (-69.1, 57.7, 10.2$ km/s, and $\mathbf{v}_S^0 = (-45.0, 45.0, 16.1)$ km/s. The positions of the LMC and SMC are indicated every 5×10^8 years by circles and squares whose size is roughly inversely proportional to distance from the viewer. The binary state here was maintained for more than 10^{10} years. As the figure shows, the minimum distance between the Galaxy and LMC often deviates about ten percent from that determined in the two-body problem in Section II. Present positions of the Clouds are indicated with filled circles and squares

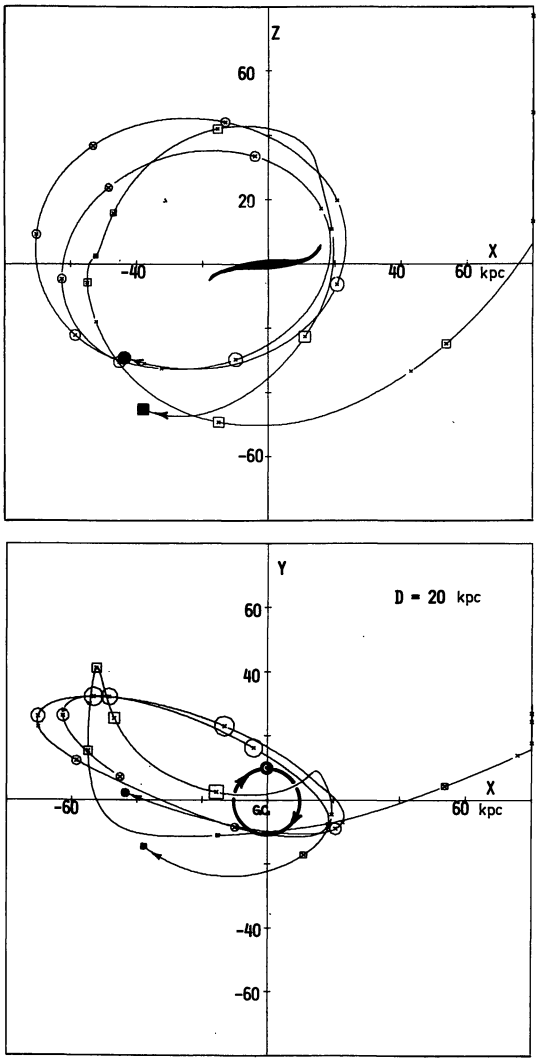

Fig. 4b. Similar to Fig. 4a, but with initial data $v_L^0=(v_L^0)_{A_3}=(-76.3, 30.6, 28.3)$ km/s and $v_S^0=(-60.0, 50.0, 26.4)$ km/s. Here the binary state is realized only for the last 2×10^9 years

velocities v_S^0 wherever v_L^0 is specified to be somewhere on the arc of the ellipse $A_{12}A_{13}\ldots A_6$ in Fig. 2. For one thing, it seems that $|v_L^0-v_S^0|$ must always be less than 70 km/s. On the other hand, when v_L^0 is picked to be one of the dark circles $A_7, A_8 \ldots A_{11}$, no capture window at all seems to exist in the (u_S, v_S, w_S)-space.

It needs hardly to be added that, since the spacings between the neighbouring points in Fig. 3 are 5 km/s in u_S and v_S, the capture windows listed in Table 3 are not mathematically strict but have the uncertainties of perhaps 5 km/s in u_S, v_S and w_S. We would not presume to guarantee that no open circles exist between the dark circles on the arc $A_7A_8 \ldots A_{11}$ in Fig. 2 or between those in the (u_S, v_S, w_S)-space in Figs. 3a and b; their existence merely seems unlikely. Our backward orbit integrations definitely show, however, that the binary structure of the LMC and SMC is easily disrupted as v_S^0 is taken distant from the capture windows.

The distribution of the open and dark circles in Figs. 3a and b and in Table 3 may perhaps be understood in the following four ways. (1) When $|v_S^0-v_L^0|$ is larger than the escape speed of the SMC from the LMC (90 km/s), the binary structure hardly needs the Galaxy to disrupt them. (2) When the LMC's orbit is relatively elongated, the LMC–SMC system seems to have less chance to be disturbed by the Galaxy. For instance the apocenter distance is 70–90 kpc for $A_{12}, A_{13}, \ldots A_6$, whereas it is only 60–70 kpc for $A_7, A_8, \ldots A_{11}$. (3) Alternatively, the permitted minima of $|v_S^0-v_L^0|$ are 20 to 70 km/s and 53 to 74 km/s, respectively, for $A_{12}, A_{13}, \ldots A_6$ and $A_7, A_8, \ldots A_{11}$. Perhaps this is instead the reason why the LMC-SMC system for the latter case is more easily disrupted by the Galactic tidal force. (4) Most important as hinted already by such classical restricted-three-body studies as those of Hénon (1965), and indeed also by the computer experiments of Pfleider (1963), is that, wherever the SMC revolves round the LMC in the same or direct sense as their shared orbital motion, it suffers a far stronger "Near-resonant" perturbation than if its revolution had been retrograde.

In their model of the "Magellanic Stream", Mathewson *et al.* (1974) have argued that the perigalactic distance D of the LMC orbit must have been at least 40 kpc in order that the binary system of the LMC and SMC have escaped tidal disruption by the Galaxy. In view of our above results, however, their conclusion that $D\geqq40$ kpc seems needlessly pessimistic.

b) $D=30$ kpc

We integrated Eq. (11) toward the past for another four thousand combinations of (v_L^0, v_S^0), on the assumption that the initial LMC velocity (u_L, v_L, w_L) is on the $D=30$ kpc ellipse in Fig. 2: we used the twelve initial velocities v_L^0 for $B_1 \ldots B_{12}$, and about three to five hundred initial velocities v_S^0 for each point B_i. Since on the average these orbits are more distant from the Galaxy, our tidal force on the LMC-SMC system is clearly smaller, and the chance that their binary structure is disrupted is correspondingly less. Indeed it emerges from computation that all points $B_1 \ldots B_{12}$ except for B_8 admit the binary structure of the Magellanic Clouds for as far back as 10^{10} years, provided v_S^0 is suitably chosen in capture windows as similar to those in Fig. 3b and Table 3. Figures 5a and b show two examples of such orbits with $D=30$ kpc.

As discussed in a), the capture windows listed in Table 3 surely involve uncertainties of about 5 km/s in u_S, v_S and w_S because of the limited number of v_S^0 adopted as initial values for the orbit integrations. For more important than those are probably the uncertainties in such basic data as the mass and size of the Galaxy, and even the relative distances of the two Clouds from the Sun. Toomre (1972) in particular has stressed that the inferred orbital period of the Clouds depends sensitively on our

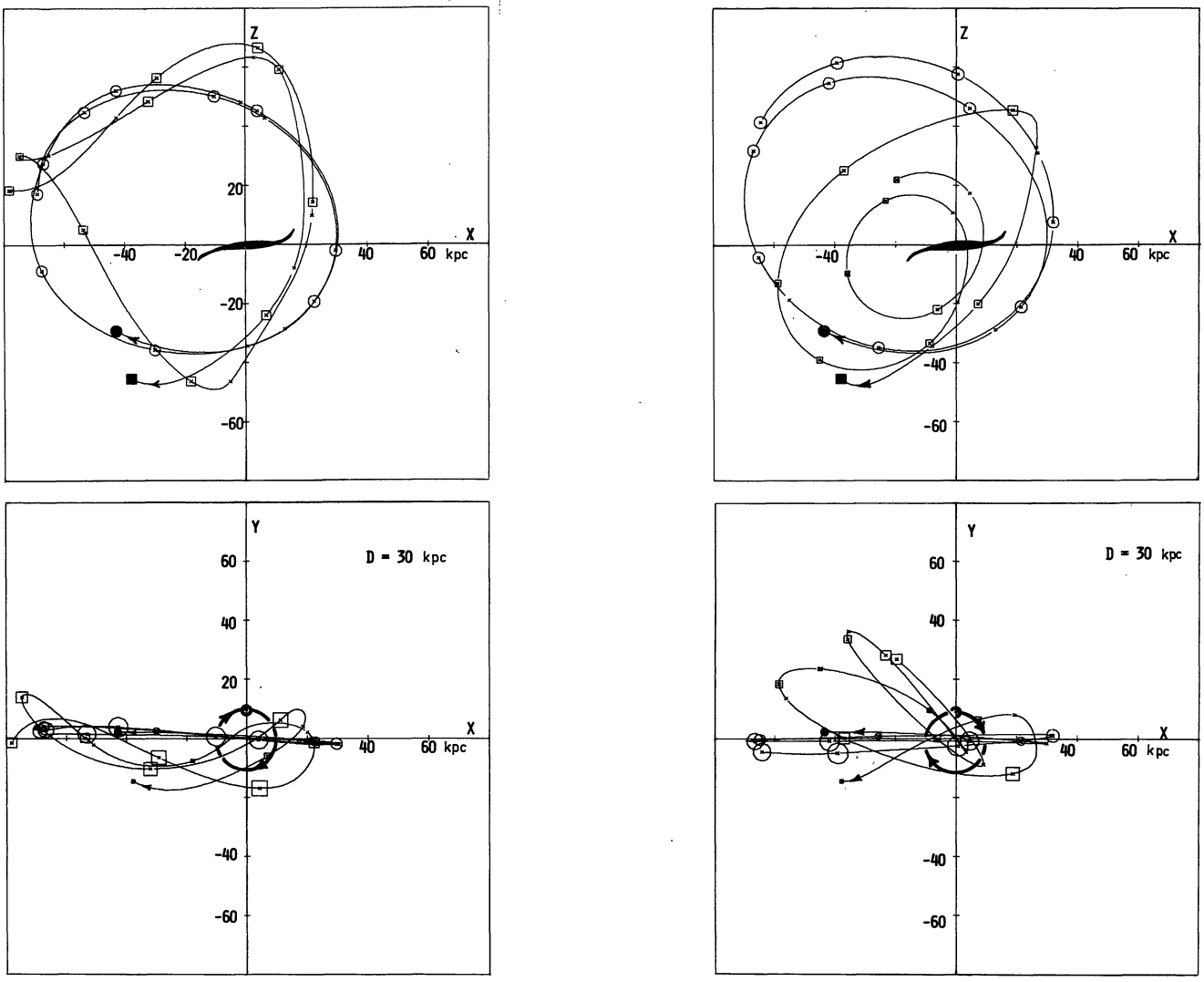

Fig. 5. (a) Sample $D=30$ kpc orbits of the LMC and SMC. The initial velocities used here were $v_L^0=(v_L^0)_{B_4}=(-80.9,\ -0.6,\ 43.7)$ km/s and $v_S^0=(-40.0,\ 30.0,\ 21.5)$ km/s; these backward integrations stop at $t=-5\times10^9$ years. (b) Similar to Fig. 5a, but $v_S^0=(-25.0,\ 0.0,\ 25.2)$ km/s. Same values of v_L^0 and period of integration

adopted speed $V_\odot$ of galactic rotation. Nevertheless, in the present explorations we will continue to employ only the parameters stated in and near Table 2.

c) $D=40$ kpc

As we remarked, Mathewson *et al.* advocated a perigalactic distance of 40 kpc or greater for the orbit of the LMC. Then even more clearly the LMC and SMC can indeed have been binary system during the past $5–10\times10^9$ years for all velocities v_L^0 on the ellipse in Fig. 2 and for suitably chosen v_S^0. Especially on the dashed part of the $D=40$ kpc curve in Fig. 2, where the LMC orbits are hyperbolic, the tidal force due to the Galaxy is negligibly small and the binary nature is easily realized and maintained. The data on just one such set of orbits, namely that corresponding to point C_4 in Fig. 2, are included in Table 3.

To summarize, from these orbit computations we can certainly state that the probability that the LMC and SMC were in a binary state for the last 5 to 10×10^9 years increases from $D=20$ to 30 to 40 kpc. In applying those results to reality, however, we can say nothing more, because there is no reason to choose the most probable value of D from only the present three-body problem. We must, therefore, introduce and make use of further material on the peculiar motions and distributions of gas and stars induced by the tidal forces of the Galaxy, LMC and SMC.

IV. Tidal Distortion of the Galaxy by the Magellanic Clouds

The close passage of the Magellanic Clouds to the Galaxy must develop large-scale distortions in the distributions of matter in each of these galaxies. Some after

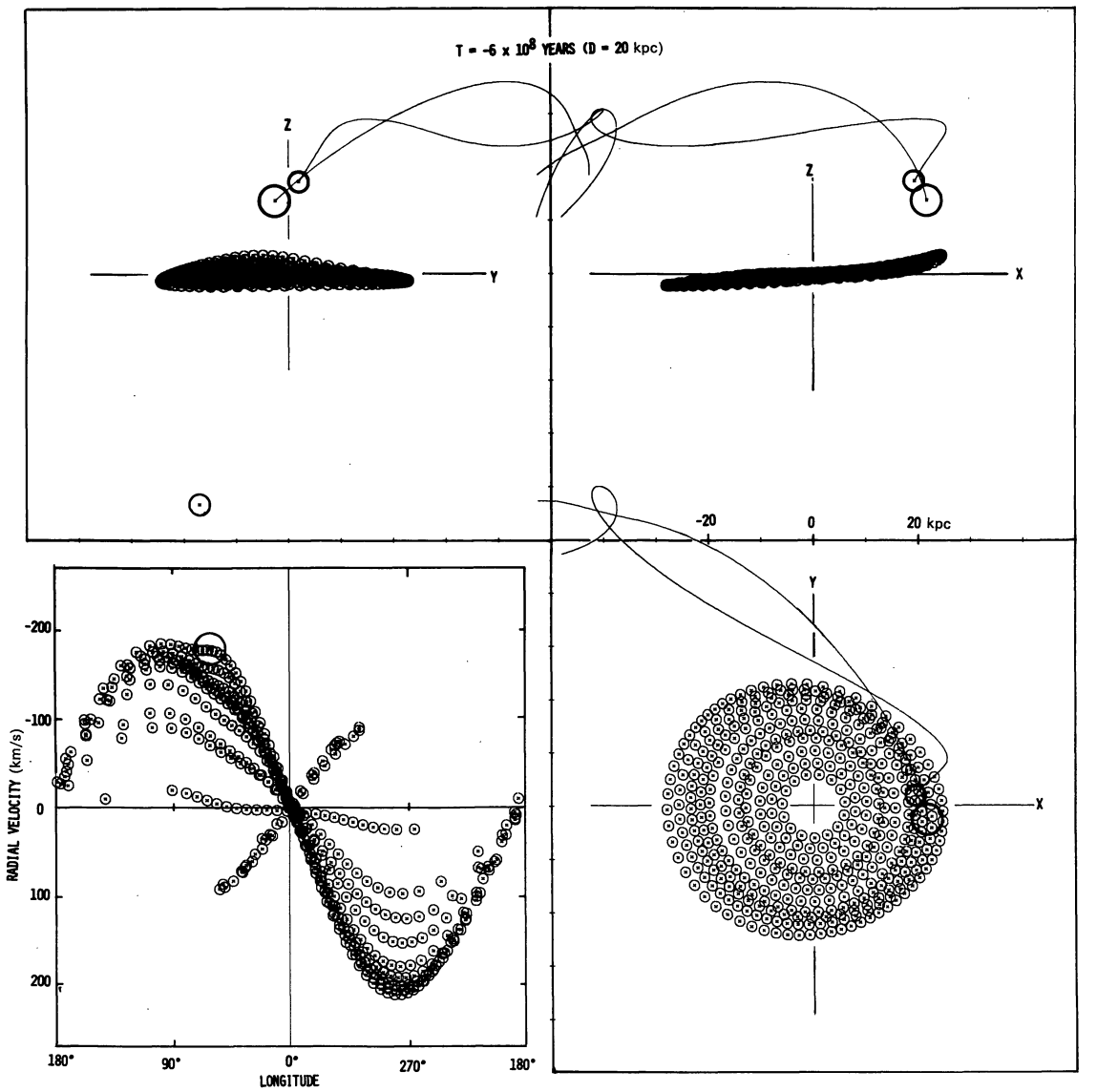

Fig. 6a. Distribution of the test particles in the Galaxy, as perturbed by the Magellanic Clouds in the $D=20$ kpc orbits given in Fig. 4a, and projected onto the (X, Y), (X, Z) and (Y, Z) planes. Here $t=-6\times10^8$ years. The longitude-radial velocity relation to be observed from the present position of the Sun, or the so-called $(l-v_r)$ diagram, is displayed also

effects should still be observable, and they should provide important evidence for determining the orbits of the LMC and SMC.

In order to estimate the distortion suffered by our Galaxy, we simulate its structure by four to five hundred test particles rotating in the potential (9) and we follow their noncircular (and nonplanar) motions caused mostly by the LMC. Our procedure closely resembles various test-particle studies by Pfleiderer and Siedentopf (1961), Pfleiderer (1963), Yabushita (1971), Clutton-Brock (1972), Toomre and Toomre (1972), Wright (1972) and Eneev *et al.* (1973). In the present paper, however, the more realistic potential (9) is adopted for the Galaxy, and forces from both LMC and SMC are taken into account simultaneously. The exploratory orbits of the LMC and SMC used in the following three subsections are taken from among those that guarantee a binary structure for the last 10×10^9 years (Section III).

The equation of motion for a test particle is then

$$\frac{d^2\boldsymbol{r}}{dt^2}=\frac{\partial}{\partial\boldsymbol{r}}\Phi_{\mathrm{G}}(\boldsymbol{r}-\boldsymbol{r}_{\mathrm{G}})-\frac{Gm_{\mathrm{L}}(\boldsymbol{r}-\boldsymbol{r}_{\mathrm{L}})}{[(\boldsymbol{r}-\boldsymbol{r}_{\mathrm{L}})^2+K_{\mathrm{L}}^2]^{3/2}}-\frac{Gm_{\mathrm{S}}(\boldsymbol{r}-\boldsymbol{r}_{\mathrm{S}})}{[(\boldsymbol{r}-\boldsymbol{r}_{\mathrm{S}})^2+K_{\mathrm{S}}^2]^{3/2}}, \tag{14}$$

where $\Phi_{\mathrm{G}}(\boldsymbol{r}-\boldsymbol{r}_{\mathrm{G}})$ is the gravitational potential (9). By definition the gravitational interaction between the test particles is negligible. The positions of the LMC and SMC, $\boldsymbol{r}_{\mathrm{L}}$ and $\boldsymbol{r}_{\mathrm{S}}$, in Eq. (14) are regarded as given functions of time.

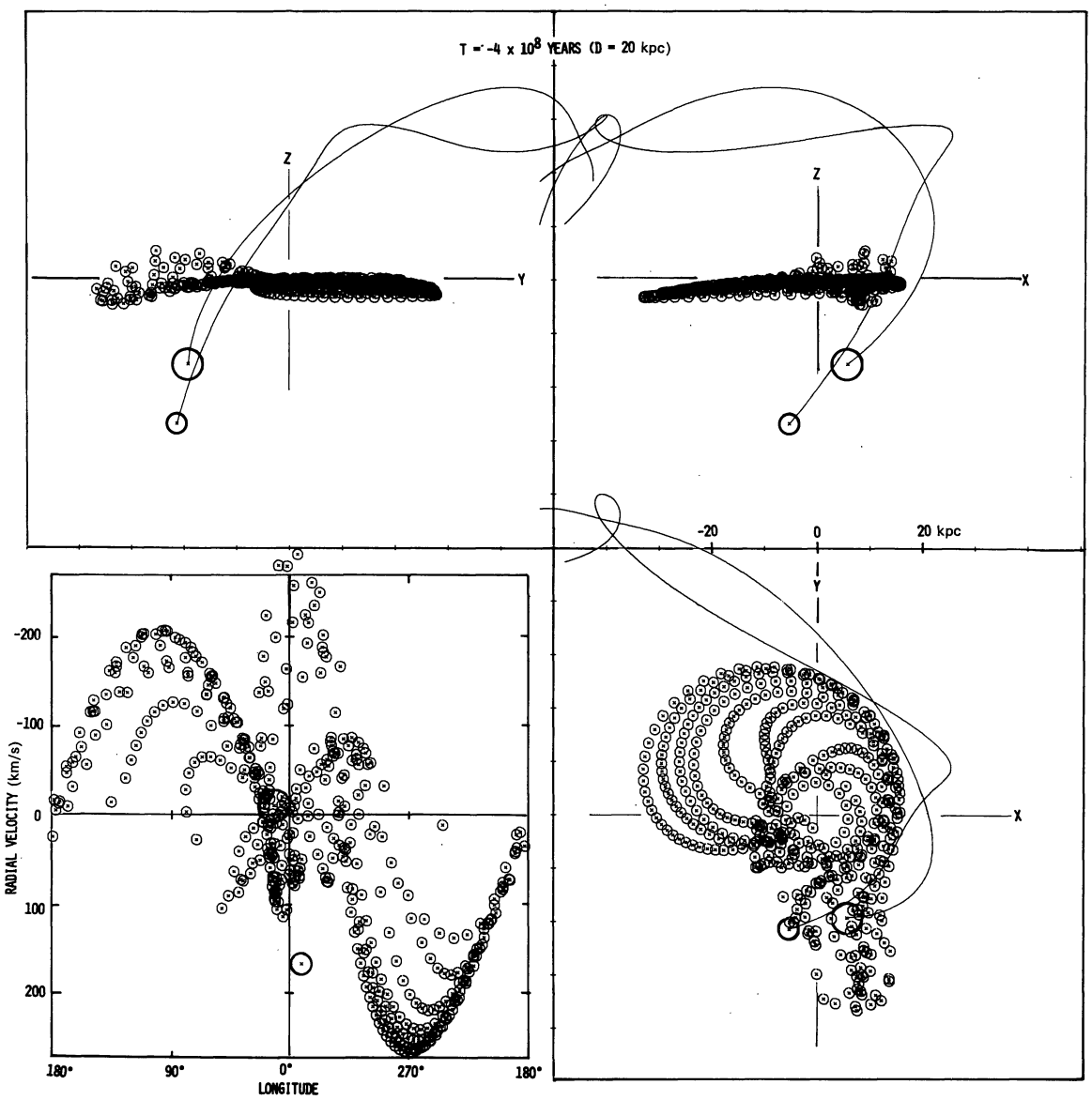

Fig. 6b. The same at $t=-4\times10^8$ years

As in the calculations of Pfleiderer, these test particles were initially located on discrete rings. Here we choose to employ eleven rings, and to place them at equally-spaced radii from $R=6$ to 26 kpc on the galactic plane. An initial circular motion was given to each particle so that the centrifugal force exactly balanced the gravitational force of the Galaxy. The present outer radius of 26 kpc is no doubt larger than most conventional values; we adopted it in order to examine also the behavior of the distant disk gas suggested by Davies (1972) and Verschuur (1973). This large choice of the edge radius greatly exaggerates most visual impressions of the damage done to the Galaxy. However, our discussion of noncircular motions and the resultant condensations of material will mainly refer to particles from original radii of 16 kpc or smaller.

Again we report separately the numerical integrations carried out for the three cases $D=20$, 30 and 40 kpc.

a) $D=20$ kpc

In the case with the pericenter distance $D=20$ kpc, the integration of Eq. (14) started, in effect, 1.7×10^9 years ago and was performed toward the present ($t=0$). Figure 6 shows the distributions of the test particles so obtained at $t=-6\times10^8$, -4×10^8, -2×10^8 and 0 years, and projected at each instant onto the (X, Y), (X, Z) planes simultaneously. (See Fig. 8a for a similar initial distribution of the test particles.) The orbits of the LMC and SMC adopted here are those given in Fig. 4a. The lower left-hand corners of Fig. 6 give the longitude radial-velocity ($l-v_r$) diagrams at each instant.

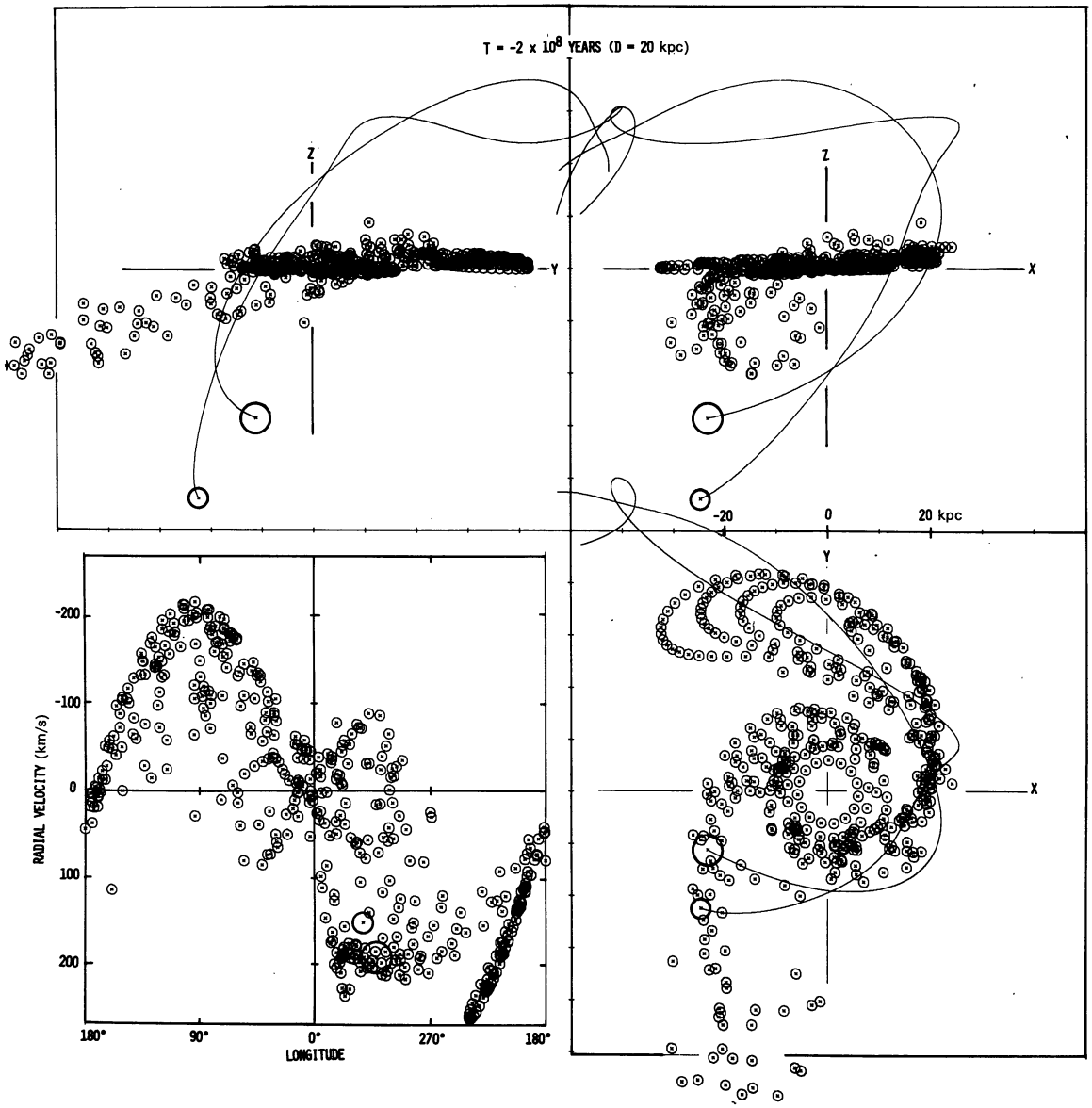

Fig. 6c. The same at $t=-2\times10^8$ years

The horizontal motion of the test particles remains almost unperturbed until the Magellanic Clouds cross the (X, Y) or equatorial plane. Then the outer particles are disturbed strongly and form two protuberances, developing into spiral arms, although somewhat asymmetric. The bending of the sheet of test particles appears slightly earlier. By $t=0$ it amounts to $\Delta Z=2$ kpc or more at $R=20$ kpc, $\Delta Z=1$ kpc at $R=15$ kpc and $\Delta Z=100$ pc even at the solar circle, $R=10$ kpc.

Unfortunately, the final noncircular velocities so induced are more than 25–30 km/s at $R=10$–15 kpc. They definitely exceed the observed H I gas motions. Also the distribution of test particles from near the solar circle, $R\simeq7$ to 13 kpc, in Fig. 7 shows how deeply the disk suffers from the tidal effects of such a close passage. Of course the same objection could be seen already in Toomre's (1970) diagram showing the violent damage expected from a tilted direct passage of the LMC in an orbit not very different from ours; in fact it was that example which caused Toomre later to favor retrograde orbits.

Similar numerical calculations to the above were carried out by us for other orbits characterized by the points A_{13}, A_{14}, ... A_3, A_4 in Fig. 2 for which the LMC and SMC have been in a binary state for at least the last 5×10^9 years. In all those cases, the LMC revolves about the Galaxy in a "direct" sense with respect to the galactic rotation or at most "over-head" (cf. Table 3). In every case there is a large tidal effect on the Galaxy usually rivaling the results in Fig. 6. However, as expected from the work of Pfleiderer and others, when the LMC orbits the Galaxy in a "retrograde" sense (A_5, A_6 and A_{12}) the

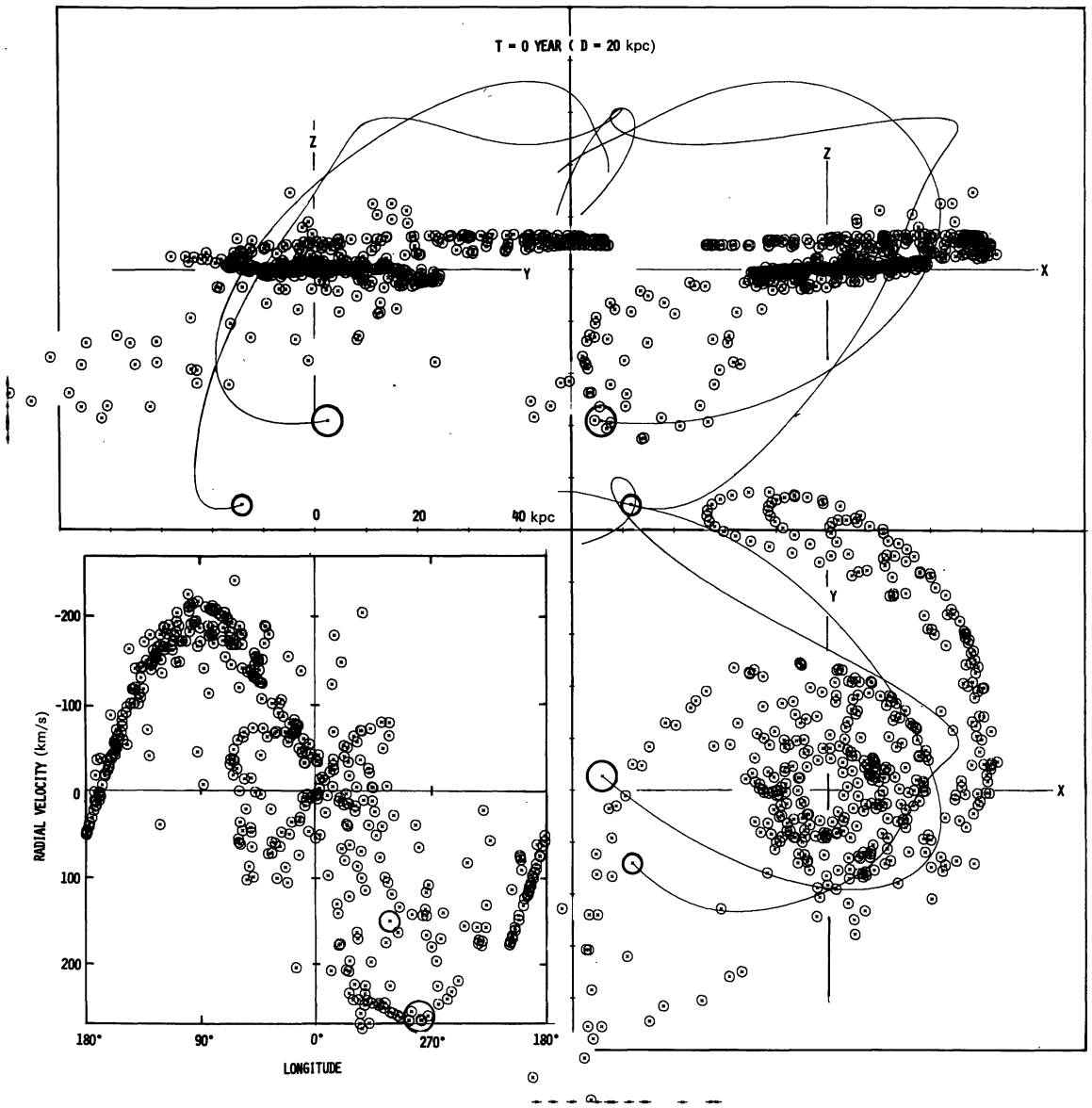

Fig. 6d. The same when $t=0$ or at present

perturbation of the particles is relatively small compared with the direct examples. The horizontal noncircular motion and resultant mass concentrations then still seem larger than the observed ones near and outside the solar circle. We computed the response of the disk for the most severely retrograde orbits like A_8 and A_9, but we do not discuss it here because the LMC and SMC could not be in a binary state for the last 5×10^9 years.

b) $D=30$ kpc

For $D=30$ kpc the test particles were initially distributed on the galactic plane in the same way as in the case $D=20$ kpc. Here numerical integrations of Eq. (14) began 1.5×10^9 years ago, and were performed forward till $t=0$.

In Fig. 8 we show the resulting distributions of the test particles projected onto the (X, Y), (X, Z) and (Y, Z) planes at $t=-15\times10^8$, -6×10^8, -4×10^8, -2×10^8 and 0 years. The orbits of the LMC and SMC adopted here are the relatively overhead ones from Fig. 5a. The $(l-v_r)$ diagrams are given also in Fig. 8.

Amplitudes of the bending are about $\Delta Z=0.01$, 0.2, 0.3 and 1 kpc respectively at $R=10$, 12.5, 15 and 20 kpc. The maximum upward and downward displacements are observed in the directions $l=100°$ to 120° and $l=270°$ to 290°, respectively. We note our reproduction of the observed north-south asymmetry of the bending: the amplitude is greater at $l=100°$ to 120° than at $l=260°$ to 290° which faces the Magellanic Clouds (Kerr and Westerhout, 1965). In so far as the amplitude and phase are concerned, the close passage at $D=30$ kpc

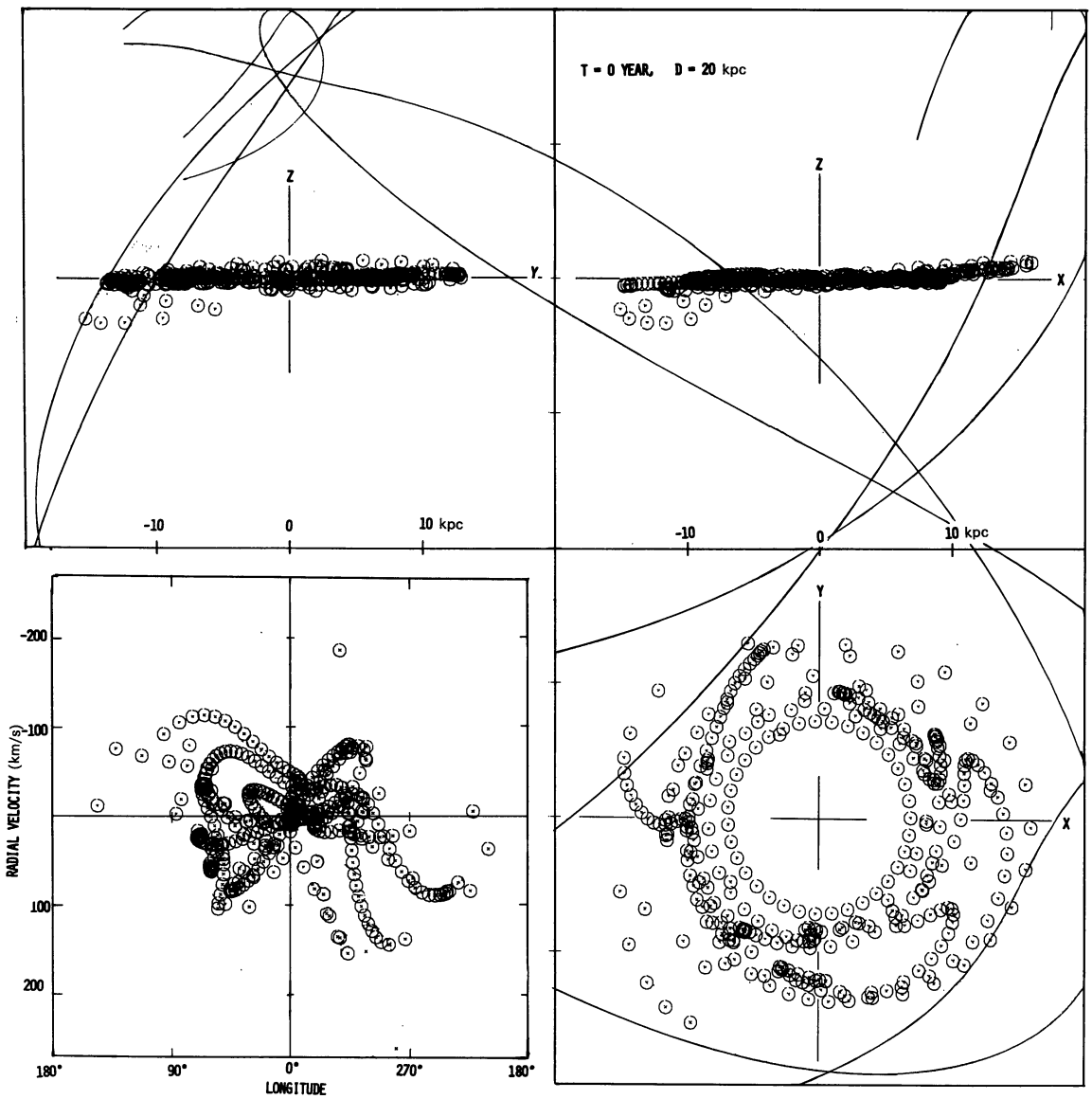

Fig. 7. The same as Fig. 6d selectively enlarged to display the final distribution of test particles near the solar circle. These test particles were initially located only on rings with radii $R=7$, 8, 9, 10, 11, 12 and 13 kpc. Too large a noncircular motion and mass condensation develope here to be compatible with observations

thus seems compatible with observations. Figure 9 gives a comparison between our results and observations of H I gas (Henderson, 1966) on the latitude-radial velocity ($b-v_r$) diagram. [In the ($b-v_r$) diagram, the reproduction of the bending is not always good. It is partly due to the adopted Innanen's model galaxy in which the rotation velocity drops rapidly outside the solar circle. If we assume more slowly decreasing rotation velocity at $r>10$ kpc, we could improve this apparent discrepancy, which we should do in our future work.]

Numerical integrations have again been made also for other orbits of the LMC: $B_1, B_2, \ldots B_{12}$ except for B_8. The well-known general trend is confirmed that a direct passage causes a stronger disturbance to the test particles than any retrograde passage. In every instance, the perturbed velocity is less than 10 km/s at the solar circle.

In these discussions of vertical distortions, we must remember that the gravitational potential of our model Galaxy was adopted beforehand and was assumed to remain unchanged during the bending of the disk. The restoring force of the bent disk upon the particles is, therefore, larger than that of a self-gravitating disk. It tends to result in underestimates of amplitudes in the present numerical studies. On the other hand, we have defined vertical amplitude as the displacement of the particles from an *invariant* plane. Yet, as Hunter and Toomre (1969) stressed the observed bending amplitude refers to a galactic disk in which the Sun is located and which itself would already have been tilted appreciably

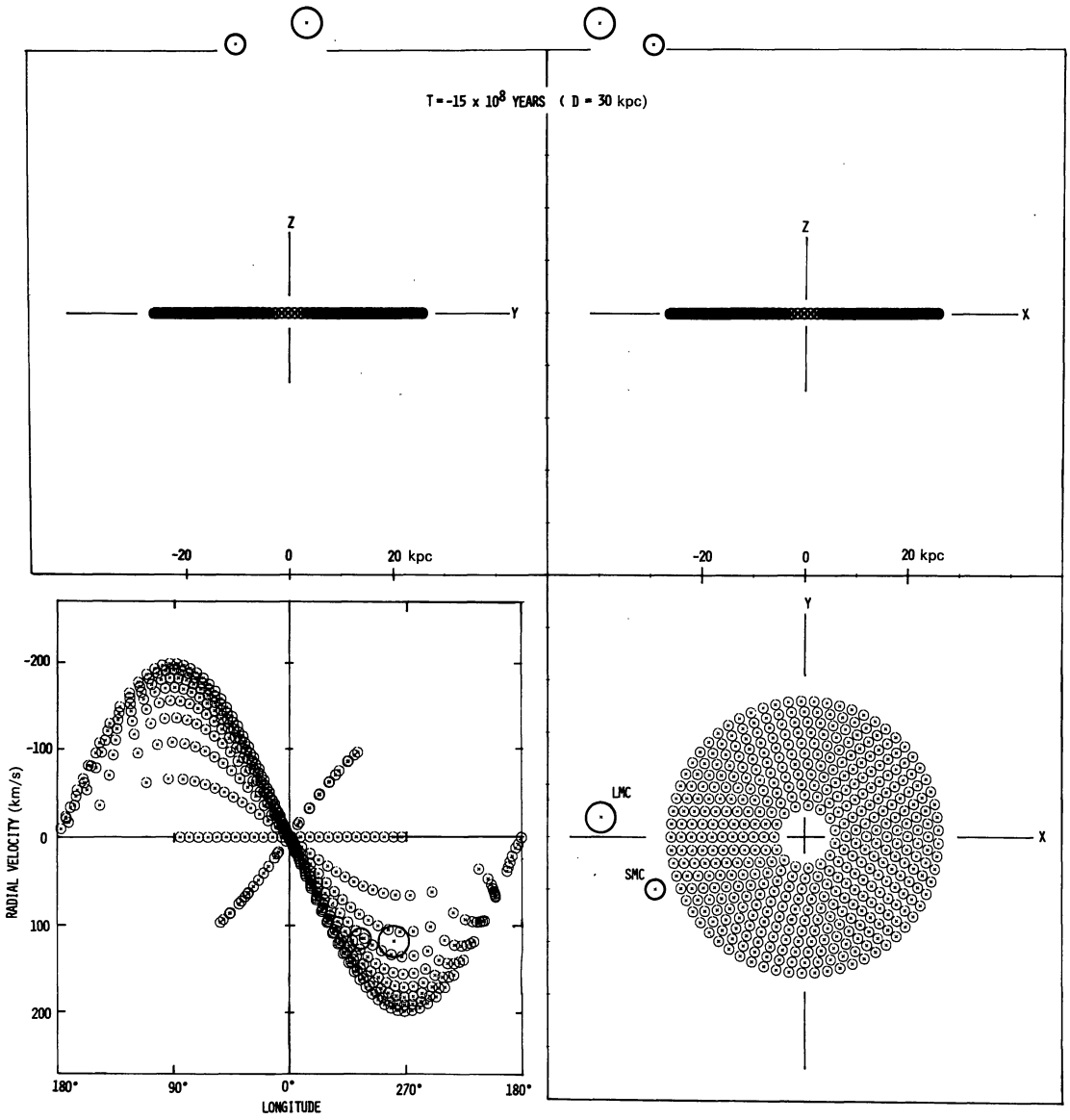

Fig. 8a. Distribution of test particles in the Galaxy, as perturbed by the Magellanic Clouds in the $D=30$ kpc orbits given in Fig. 5a. Here $t=-1.5\times10^9$ years, or the figure shows the initial locations of the galaxies and test particles

by the tidal force from the LMC. For this reason, the vertical displacement obtained for our test particles tend to exaggerate the true (i.e., differential) bending.

Thus it is not a simple matter to decide which passage distance is more realistic, $D=20$ kpc or $D=30$ kpc, by comparing only the computed bending with the observations. All we can say on that basis is that D lies probably somewhere between 20 kpc and 30 kpc. However, taking into account equally the bending and the horizontal damage to the disk, we suspect that $D=30$ kpc is more compatible with observations than $D=20$ kpc. Later we will provide more evidence to support this impression.

c) $D=40$ kpc

The initial distribution and rotation velocity of the test particles were the same as before. Numerical integrations of Eq. (14) now started 2×10^9 years ago, using only the single pair of LMC/SMC orbits designated as C_4 in Fig. 2 and Table 3. The resulting distributions of the test particles and the $(1-v_r)$ diagram show much too small an amplitude of the bending: $\Delta Z=0.05$, 0.1 and 0.3 kpc at $R=10$, 15 and 20 kpc, respectively. (Also the phase of the bending is in disagreement with observations, but this criticism may refer only our particular choice of the Cloud orbits.)

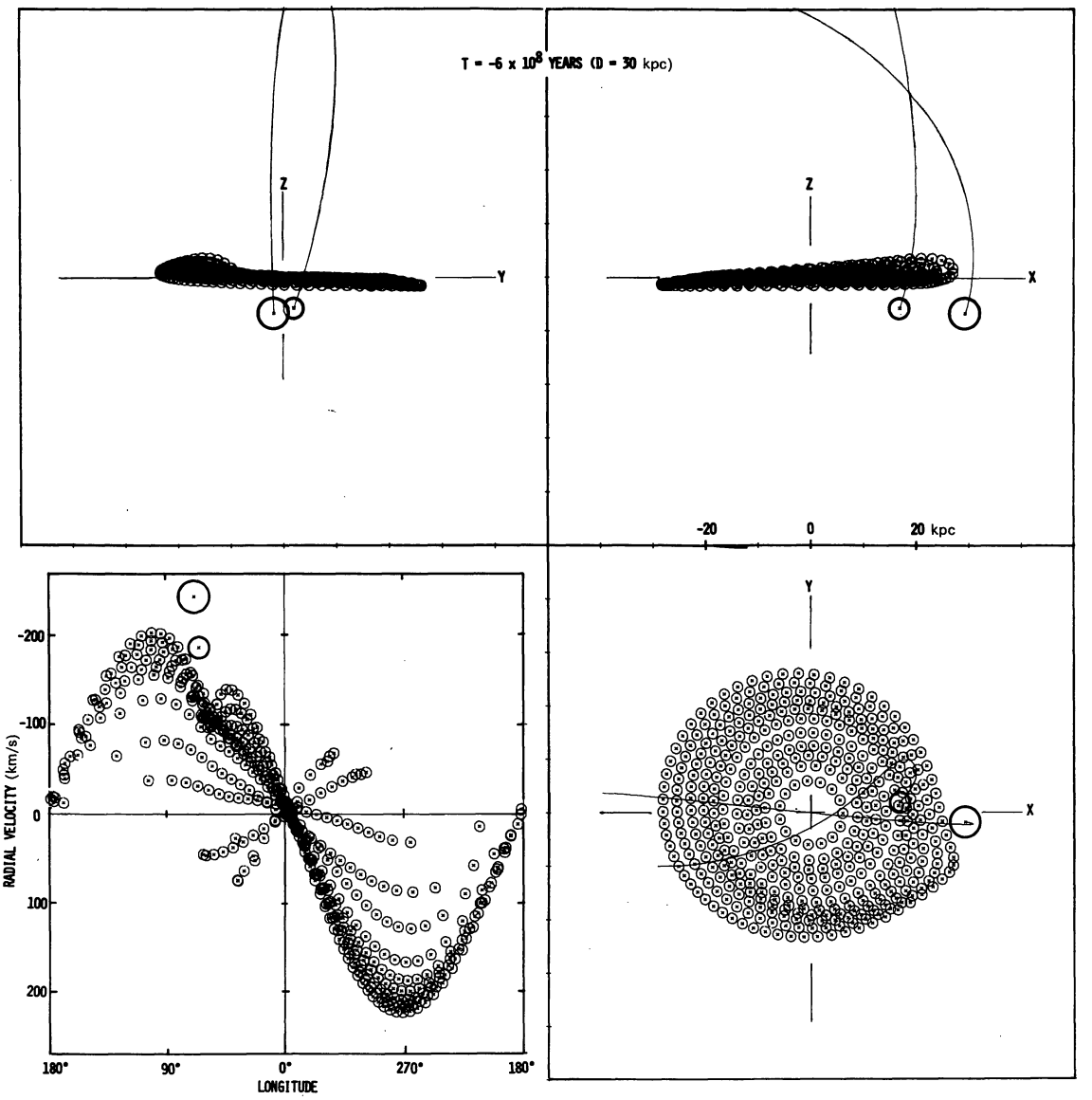

Fig. 8b. The same at $t = -6 \times 10^8$ years

If we are to search for the mechanism of the bending in a tidal interaction between the Galaxy and the Magellanic Clouds, it thus seems that we must rule out from our discussions all cases with $D \geqq 40$ kpc.

V. Tidal Effects of the Galaxy on the Magellanic Clouds

We turn our attention, next to the dynamical behavior of matter in and around the LMC and SMC under the tidal force of the Galaxy. As cited in Mirabel and Turner (1973), Toomre predicted, based on his own test particle computations, that the outer parts of the Magellanic Clouds (and especially the SMC) should have been disrupted during the close passage of the Galaxy, and their debris would make a long streak of gas in the vicinity of the Clouds. According to his suggestion, Mirabel and Turner searched for such a hydrogen streak from the Magellanic Clouds, though with a negative result. However, more extensive observations by Mathewson *et al.* (1974) have recently revealed the existence of a pronounced "Magellanic Stream" of hydrogen gas emerging from the Clouds. It forms an approximate great circle on the sky, running past the galactic poles and through the high-velocity H I cloud region near $l = 120°$, $b = 40°$. This stream of gas may conceivably be what Toomre asked for before theoretically.

In the present section we aim to reexamine such dynamics of the interstellar material from the Clouds, with special regard to reproducing the "Magellanic Stream" and in attempt to select more probable orbits of the LMC and SMC out of the large number of candidate orbits de-

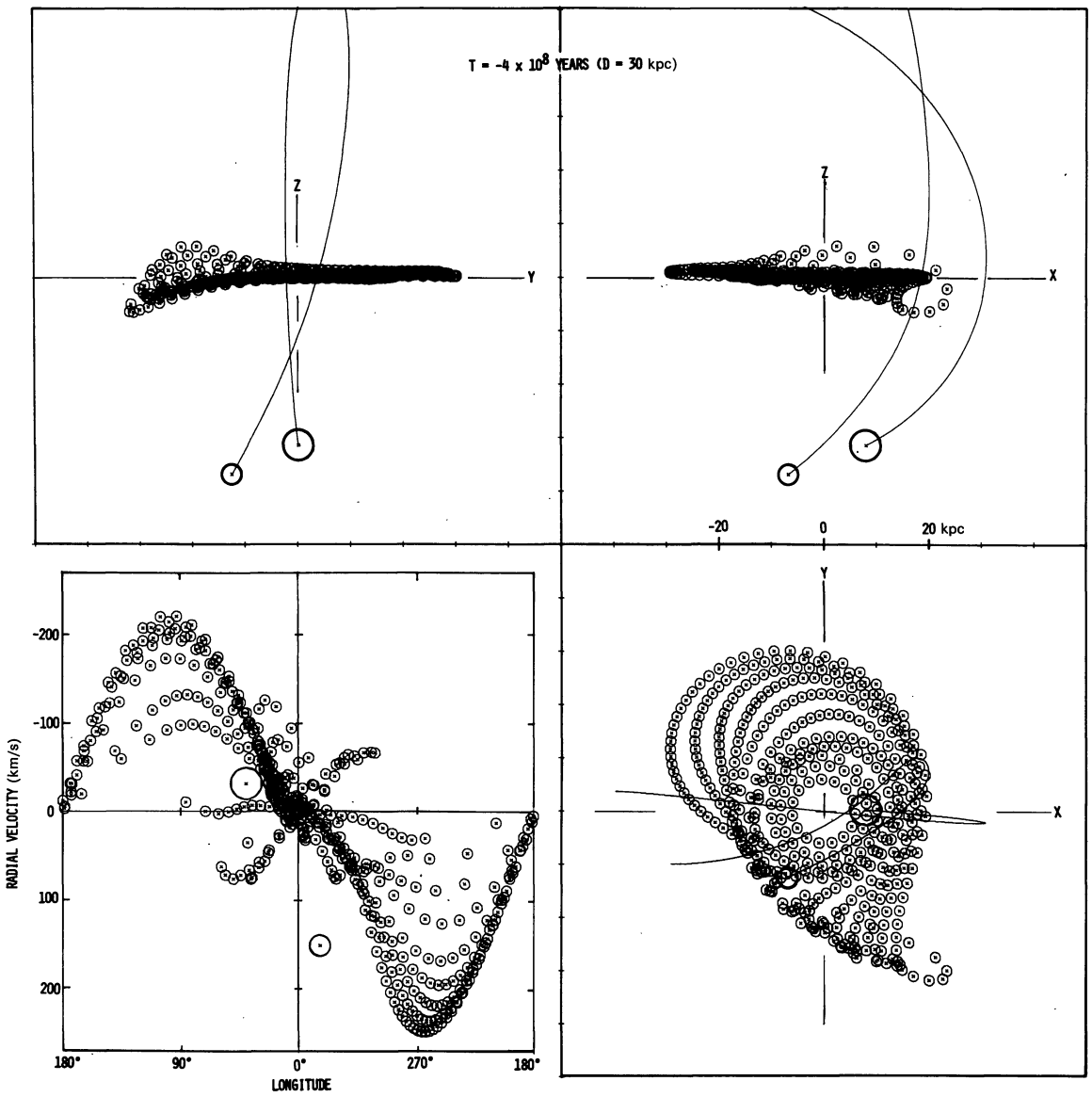

Fig. 8c. The same at $t=-4\times10^8$ years

termined in the preceding sections. For this purpose, we distributed more than two hundred test particles in each of the LMC and SMC. They were placed initially on eleven rings with radii 1–11 kpc around the center of the LMC and on eight rings with radii 1–8 kpc around the SMC. Again, rotation was given to the test particles, so that the centrifugal force balanced the gravitational force in each of the Clouds.

From the ratio of the major and minor axes of the LMC, de Vaucouleurs (1960) estimated an inclination angle $i=27°$ between the line of sight and the rotation axis of the LMC. This rotation plane of the LMC is nearly parallel to our $y-z$ plane, differing only about 7°. According to de Vaucouleurs, the rotation is clockwise as seen from the x-axis. In our numerical calculations the initial rotation plane of the LMC particles was taken to be exactly parallel to the $y-z$ plane. We also assumed at the initial epoch of our numerical integrations that even the SMC rotated parallel to the same plane, and in the same clockwise direction as the LMC. The orbits of the LMC and SMC chosen for the following three subsections all guarantee a binary state for the last 5×10^9 years.

a) $D=20$ kpc

With $D=20$ kpc, numerical integrations of Eq. (14) for the test particles in the LMC and SMC began 1.7×10^9 years ago, at which time the LMC was at the apogalacticon; as before, they were performed forward to $t=0$.

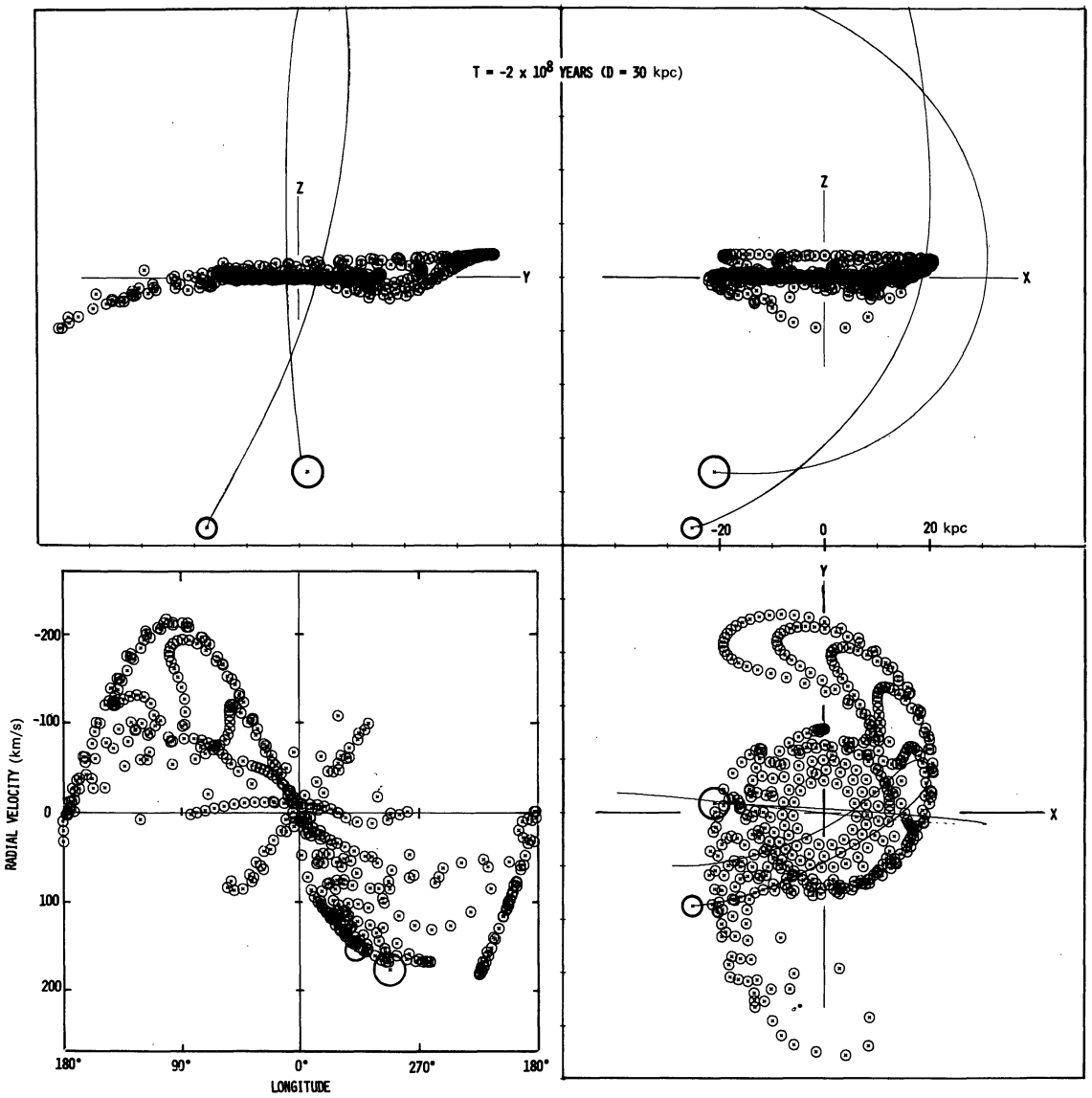

Fig. 8d. The same at $t=-2\times10^8$ years

In this example, our rather extensive SMC undergoes a strong disruption by the tidal force of the LMC, well before those two systems pass near the Galaxy. A small portion of the test particles remains bound gravitationally to the SMC. On reaching the perigalacticon, a significant number of these particles is pulled out in turn, and make a tail behind the LMC and SMC. In order to see whether such debris can form a narrow band on the sky like the Magellanic Stream, we plotted the positions of the test particles on the (l, b)-plane (Fig. 10a), together with the Magellanic Stream. The pulled-out particles are too scattered to form a narrow band.

Similar computations were also carried out for other cases A_1, A_4, A_6, A_{12} and A_{14} on $D=20$ kpc ellipse (Fig. 2) in which the LMC and SMC could be a binary for the last 5×10^9 years if v_S^0 is properly chosen. All of the particle distributions for these five cases reveal still scattered features, not reproducing a narrow band.

If we take a view point that the Magellanic Stream was produced by neutral hydrogen gas out of the LMC and SMC, it seems therefore better to rule out the case of $D=20$ kpc again from the model of the close passage of the Magellanic Clouds.

b) $D=30$ kpc

In the case of a passage at the intermediate distance, $D=30$ kpc, the initial conditions for the test particles are the same as in a). Integrations here began 1.5×10^9 years ago. Figure 11 shows the dynamical evolution of the test particles in the LMC and SMC, whose B_4 orbits are given in Fig. 5a. The disruption of the LMC and

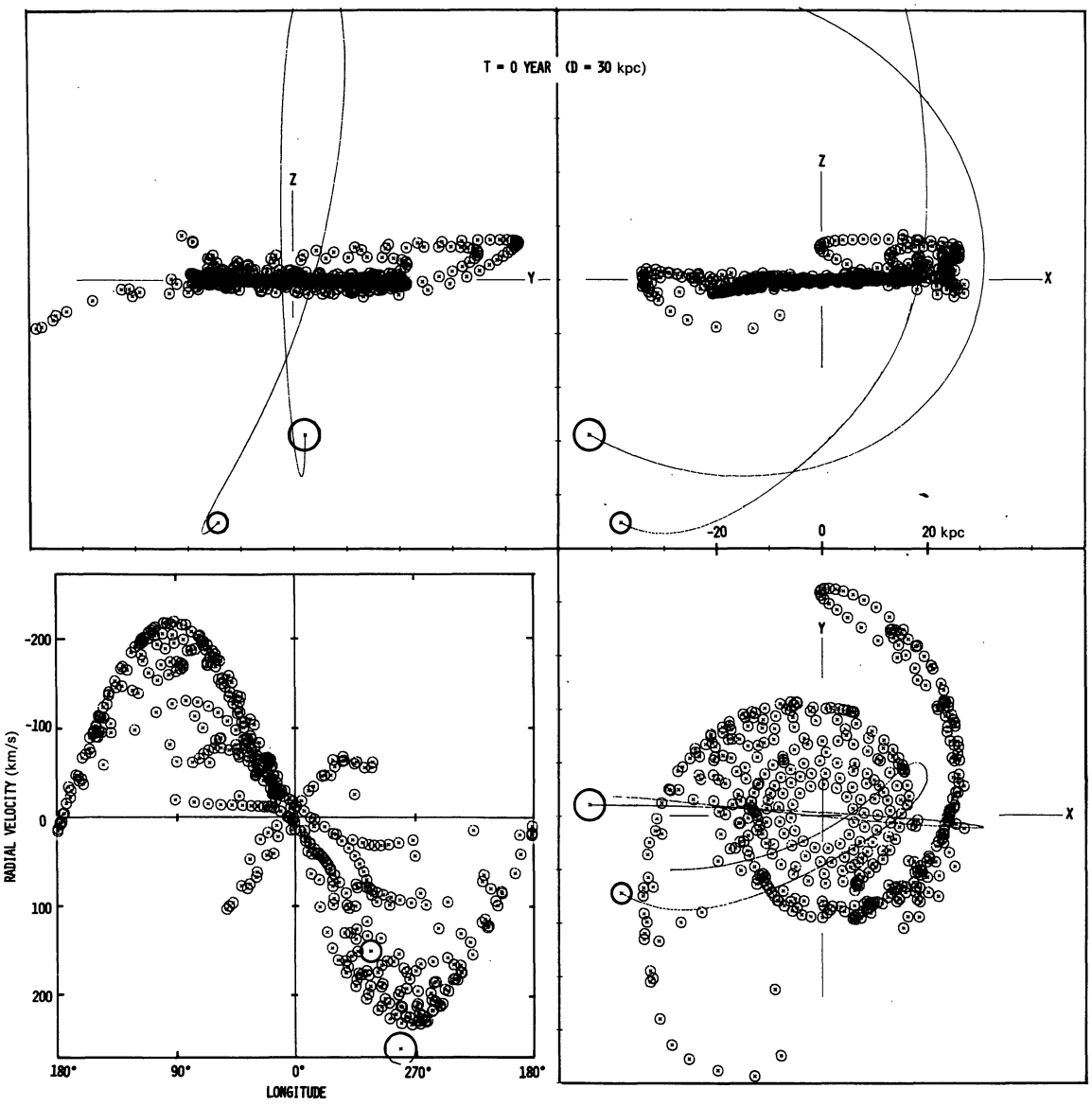

Fig. 8e. The same when $t=0$ or at present. This result is used in discussing the north-south asymmetry of the rotation curve (see Fig. 13)

SMC is observed as in case $D=20$ kpc. When the LMC and SMC approach the perigalacticon, their tidal disruption is enhanced and many more particles are pulled out, making a tail behind them.

The positions of the particles at $t=0$ are plotted on the (l, b)-plane in Fig. 10b. The pulled-out particles fall roughly on a great circle on the sky running through the LMC, SMC and the points $(l, b)=(120°, 0°)$ and $(0°, -80°)$, almost like the Magellanic Stream.

The model of $D=30$ kpc can simulate also the well-known high-velocity gas clouds if our test particles are regarded as diffuse hydrogen gas: the gases with radial velocity of about -150 km/s at $(l, b)=(120°, 30°)$ and those with $+100$ km/s at $(270°, 0°)$ referred to the LSR. The typical life-time of these feature against smearing out in space is about 10^9 years.

At the close passage, many particles are pulled out of the LMC and SMC, but some particles remain from the disruption. The Cloud region is thus enlarged on the (l, b)-plane of Fig. 12, where the particle distribution at $t=0$ has been superposed on the observed hydrogen distribution. We find that a bridge linking the two Clouds, a tail extending toward the galactic south pole and a sharp boundary of H I gas distribution at $(l, b)=(285°, -25°)$ to $(270°, -33°)$ are all mimicked reasonably well.

Unfortunately, all is not well with this model. According to Mathewson *et al.* (1974), the radial velocities within the stream at $(l, b)=(0°, -80°)$ through $(90°, -30°)$ are -100 to -200 km/s referred to the non-rotating Galaxy. These large velocities of approach cannot be reproduced at all well by the present model: we find

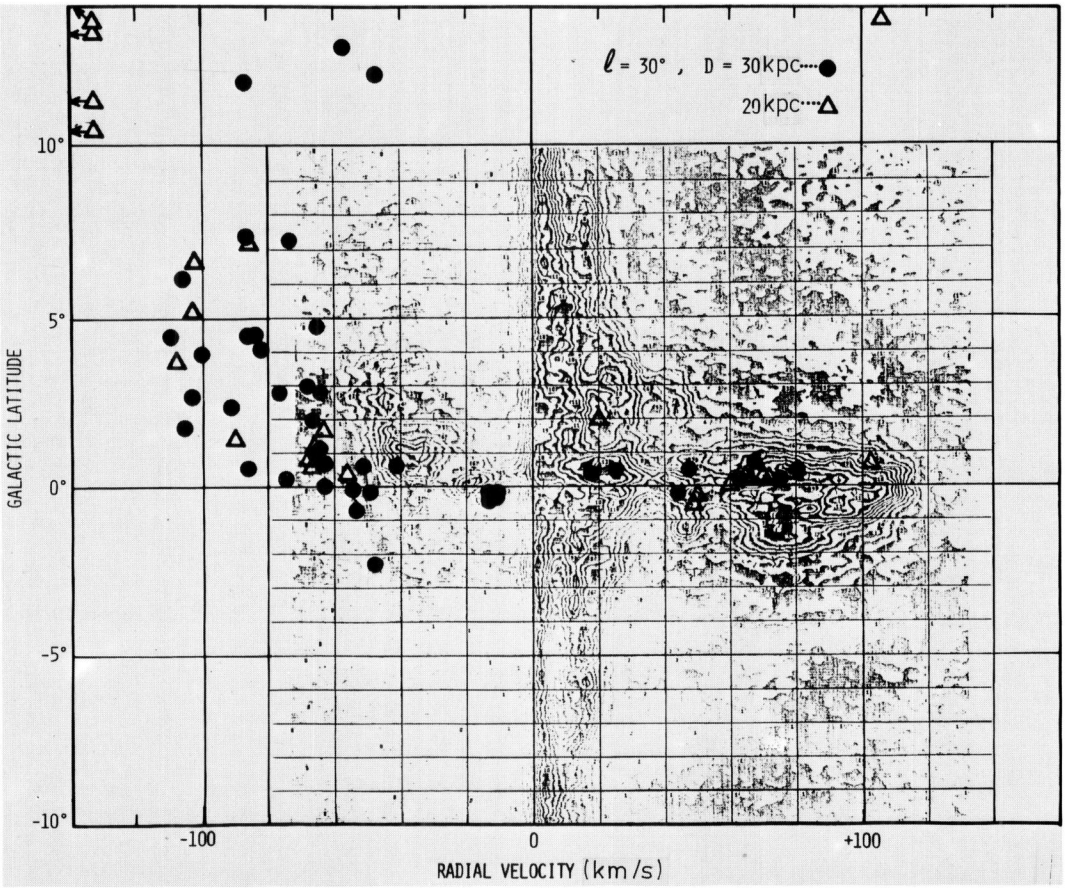

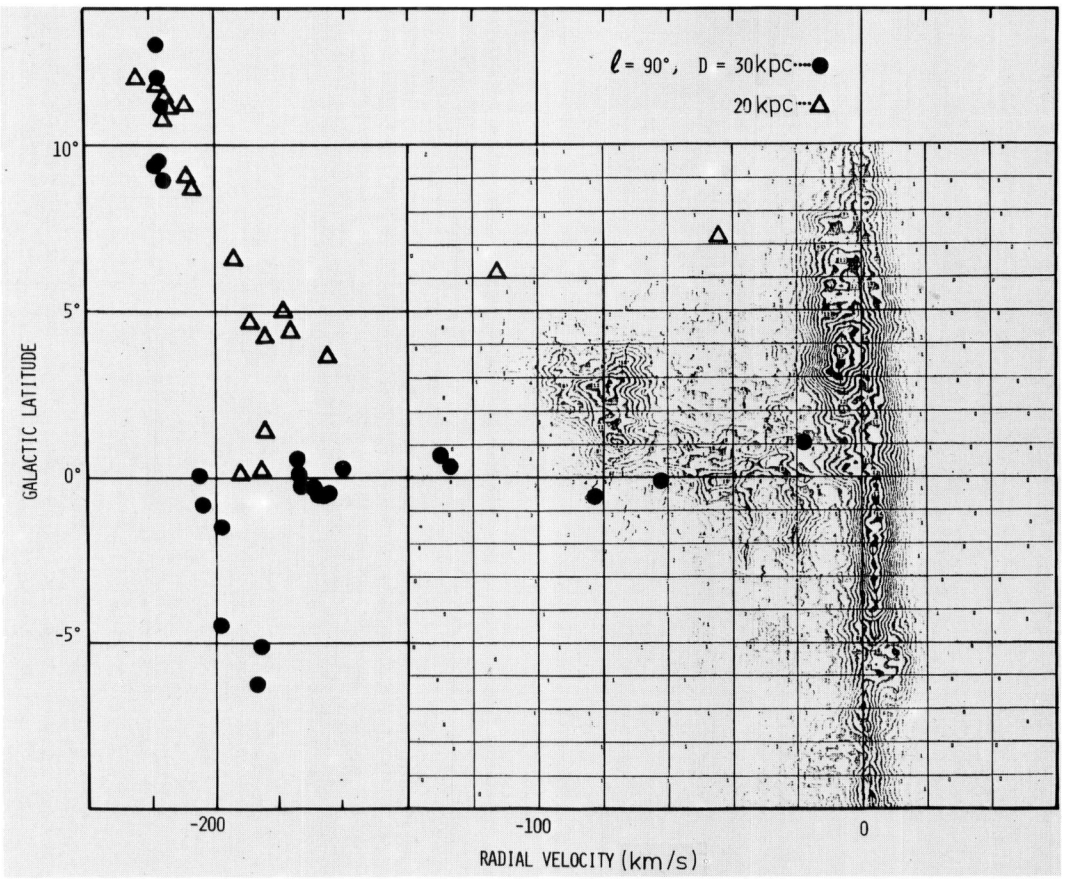

Figs. 9a and b. The computed and observed bendings of the galactic disk on the latitude-radial velocity diagrams at $l = 30°$ and 90°. The dark circles and open triangles correspond to the situation portrayed in Fig. 8e ($D = 30$ kpc) and with Fig. 6d ($D = 20$ kpc), respectively. The observation is due to Henderson (1966). Some qualitative agreements are found ($l = 30°$), but they are not very satisfactory. This may be due to the rotation curve adopted from Innanen's (1966) model 10-252 which decreases rapidly with outside the solar circle

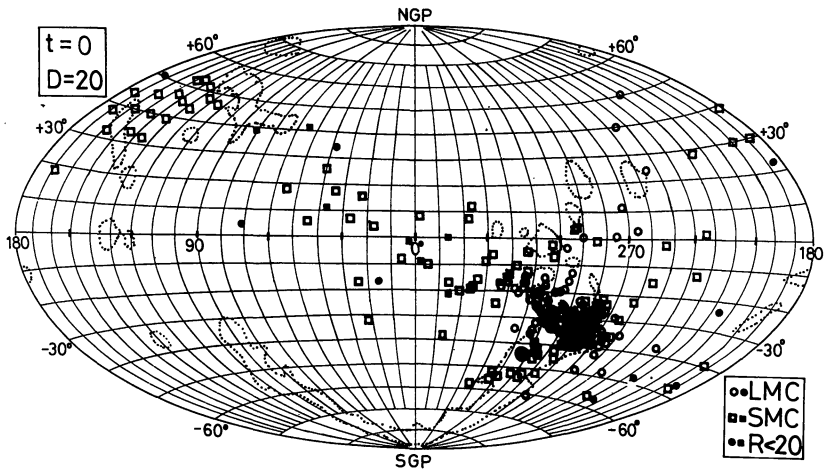

Fig. 10a. Present ($t=0$) distribution of the test particles in the LMC and SMC on the (l, b) plane in the $D=20$ kpc orbits given in Fig. 4a. The particles pulled out of the LMC and SMC are much scattered on the sky. Dotted lines enclose the observed H I high-velocity clouds and the "Magellanic Stream" (Mathewson *et al.*, 1974). ○: particles which were initially in LMC, and □: in SMC

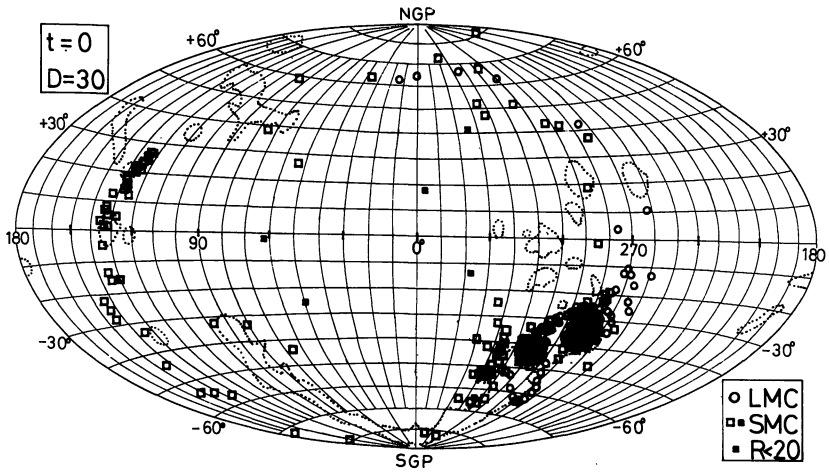

Fig. 10b. Similar to Fig. 10a but in the $D=30$ kpc orbits given in Fig. 5a. The pulled-out particles roughly fall on a great circle on the sky, almost like the "Magellanic Stream". They also well simulate the high-velocity clouds. Particles with smaller circles and squares are "stragglers" from the LMC and SMC, namely those whose galacto-centric distances are less than 20 kpc

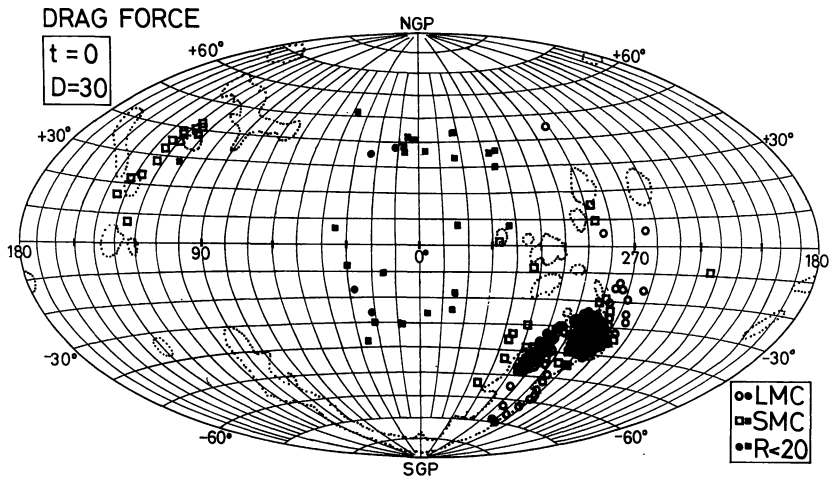

Fig. 10c. Similar to Fig. 10b with the $D=30$ kpc orbit in Fig. 5a but here the drag force on the test particles is taken into account. The large negative velocities observed within the Magellanic Stream at $(l, b)=(90°, -30°)$–$(0°, -80°)$ cannot be reproduced in this case, too

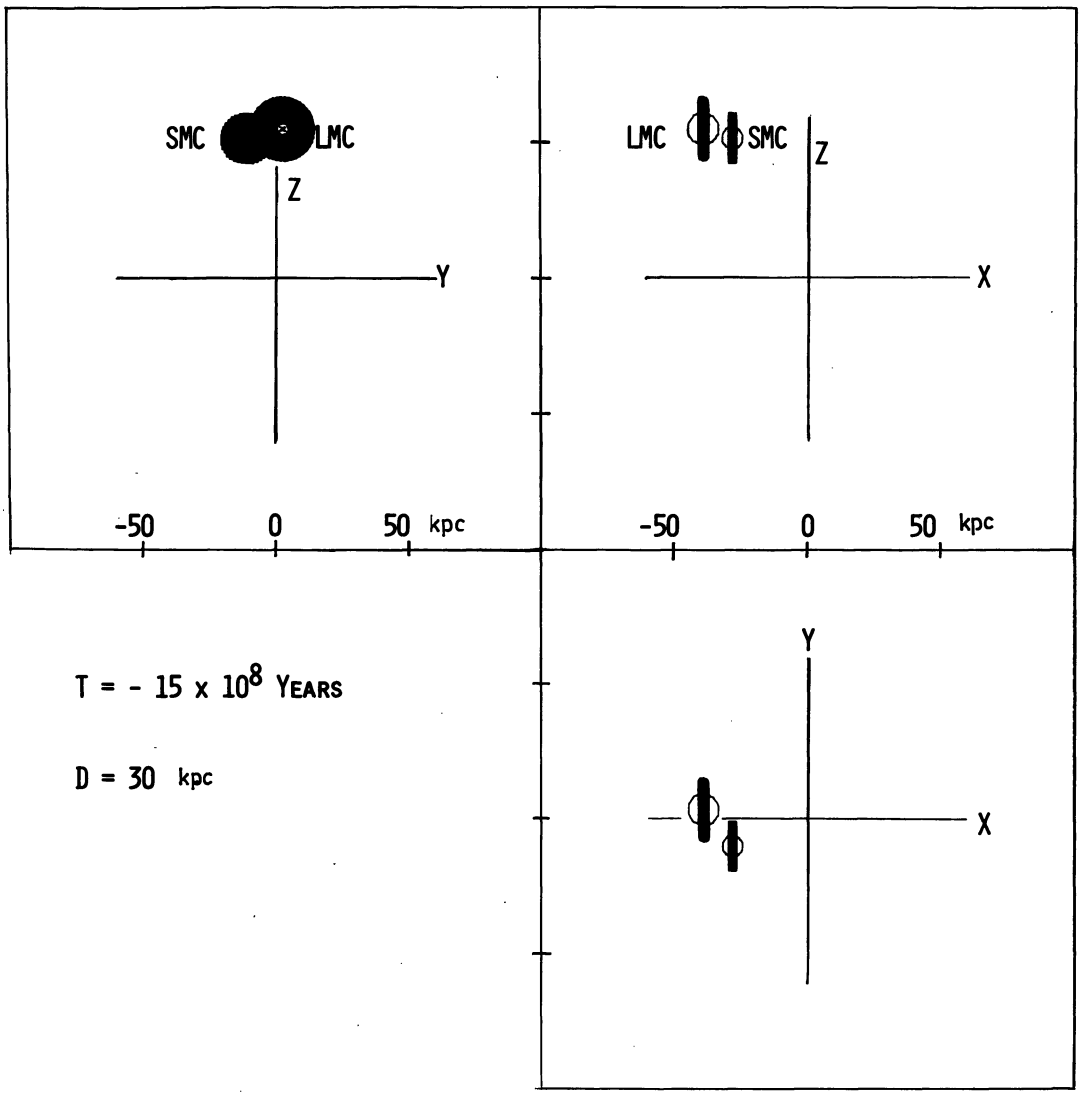

Fig. 11a. Dynamical evolution of the test particles around the LMC and SMC projected onto the (X, Y), (X, Z) and (Y, Z) planes. In the $D=30$ kpc orbits given in Fig. 5a. Here $t=-1.5\times10^9$ years, or the figure shows the initial locations of the galaxies and test particles

instead that such simulated line-of-sight speeds near $(l, b)=(90°, -30°)$ are roughly -20 to 0 km/s. For similar reasons, already Oort (cited by Mathewson *et al.*) suggested a drag force due to the intergalactic gas. Figure 10c shows the distribution of test particles which move under both gravity and drag force of the form $-k\boldsymbol{v}$, with $k=1.0\times10^{-9}$ (years)$^{-1}$. No acceptable result was, however, obtained for a wide range of $k=0.01$–3×10^{-9} (years)$^{-1}$.

Nevertheless, it is unclear to us yet whether this velocity objection is entirely devastating. We are certainly struck by the fact that, apart from this one difficulty, the $D=30$ kpc model in Fig. 10b seems to reproduce the Magellanic Stream fairly well. From the direction of the tail and the geometry of the observed great circle, we can select the orbits B_3, B_4 and B_5 as the most probable ones out of B_1 to B_{12} for most of which the same test particle computations were carried out. These orbits (B_3, B_4 and B_5) are all nearly "overhead" ones, with the last crossing of the Galactic plane having occurred roughly at longitude $l=60°$, as viewed from the present location of the sun.

We have adopted 11 kpc and 8 kpc, respectively, for the outermost radii of the rings in the LMC and SMC. If they were less than 5 kpc in the LMC and 2 kpc in the SMC, no particle was pulled out and no tail was formed. We must, therefore, consider that hydrogen envelopes greater than these radii were already present before they pass the perigalacticon.

The same numerical integrations were carried out starting both earlier and later than $t=-1.5\times10^9$ years. In every case, a band of the test particles similar to the Magellanic Stream could be reproduced roughly along a great circle on the sky. Although much more scattered when the integration was started earlier ($t\lesssim-2\times10^9$ years). The reproduction of the high-velocity H I clouds at $l\simeq120°$, $b\simeq50°$ was improved. We note that the geometry of the great circle of the particles on the sky is determined primarily by the inclination angle i of the

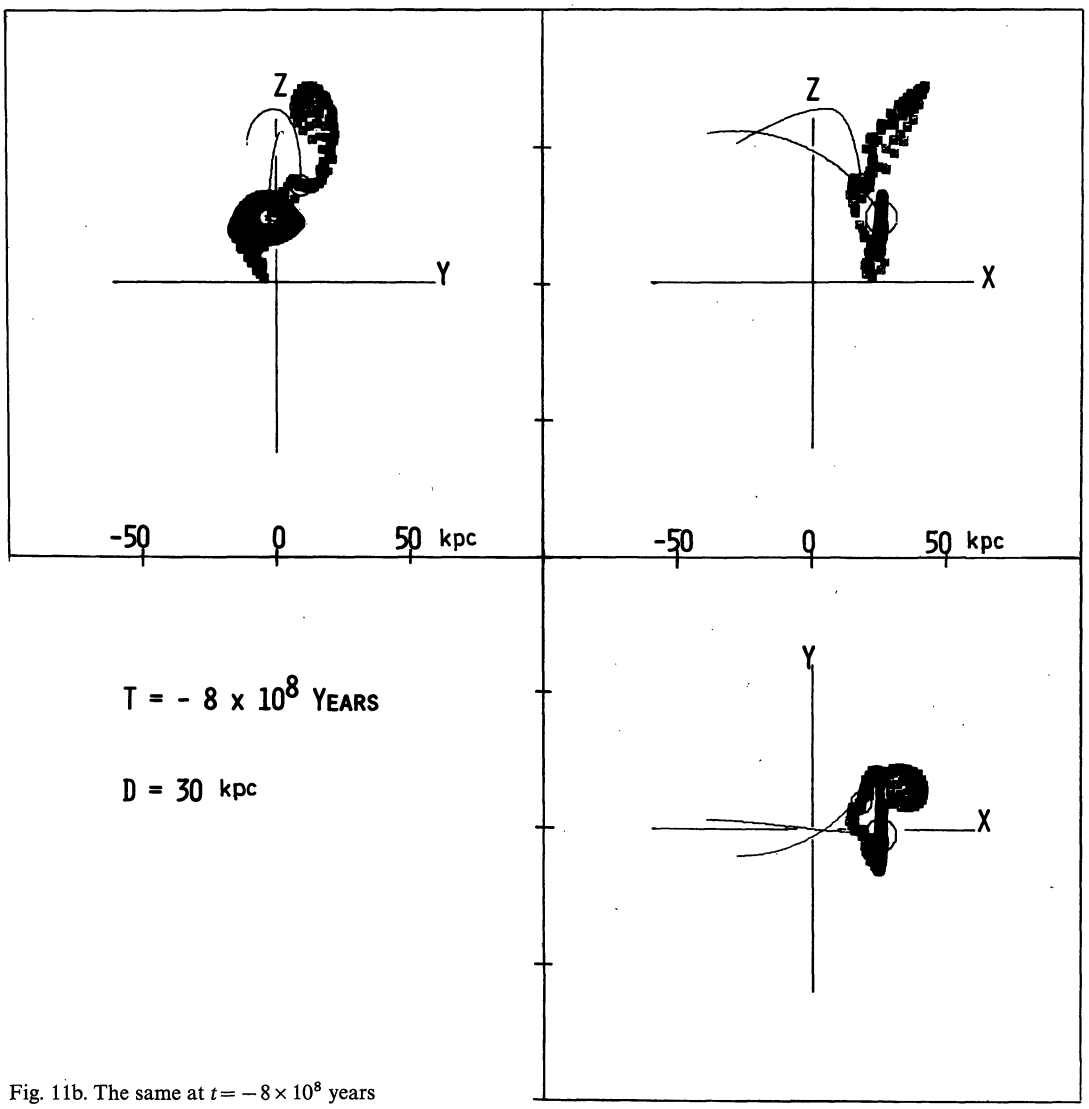

Fig. 11b. The same at $t=-8\times10^8$ years

orbital plane of the LMC, but it is not greatly affected by the initial time of the integration.

c) $D=40$ kpc

The tidal disruption of the LMC and SMC during the passage near the Galaxy is observed, but the pulled-out particles produce neither the narrow band on the sky nor the high-velocity clouds. The model of $D=40$ kpc seems to be ruled out in the present section, too, if we take the view point that the Magellanic Stream is due to the gaseous debris extracted tidally from the Magellanic system.

VI. Conclusions and Comments

We have obtained some orbits of the LMC and SMC along which they were in a binary state at least for the last 5×10^9 years—and often the whole 10^{10} years—, and are now at their present positions with the observed radial velocities. The binary structure is shown to escape tidal disruption even at passages within a distance of 20 kpc from the galactic center, provided the SMC orbit is carefully chosen. We have simulated the structure and evolution of the Galaxy, LMC and SMC by numerically following the motion of two to five hundred test particles initially distributed in circular disks within each of them. If both the bending of the galactic disk and the Magellanic Stream are due to the gravitational interaction among the Galaxy, LMC and SMC, the most reasonable orbits of the LMC seem to be as follows: The pericenter and apocenter distance are 30 kpc and 80 kpc, and the inclination angle is roughly $i=70°$ to 110°, with the ascending and decending nodes at $l=280°$ and 55°, respectively, when $i\approx90°$. The perigalacticon occurs at $(l, b)=(65°, -40°)$ for $i\approx90°$. The Magellanic Stream is a transient feature with a time-scale of 10^9 years.

According to the current density-wave theory (cf. Lin *et al.*, 1969), the spiral arms are formed and maintained

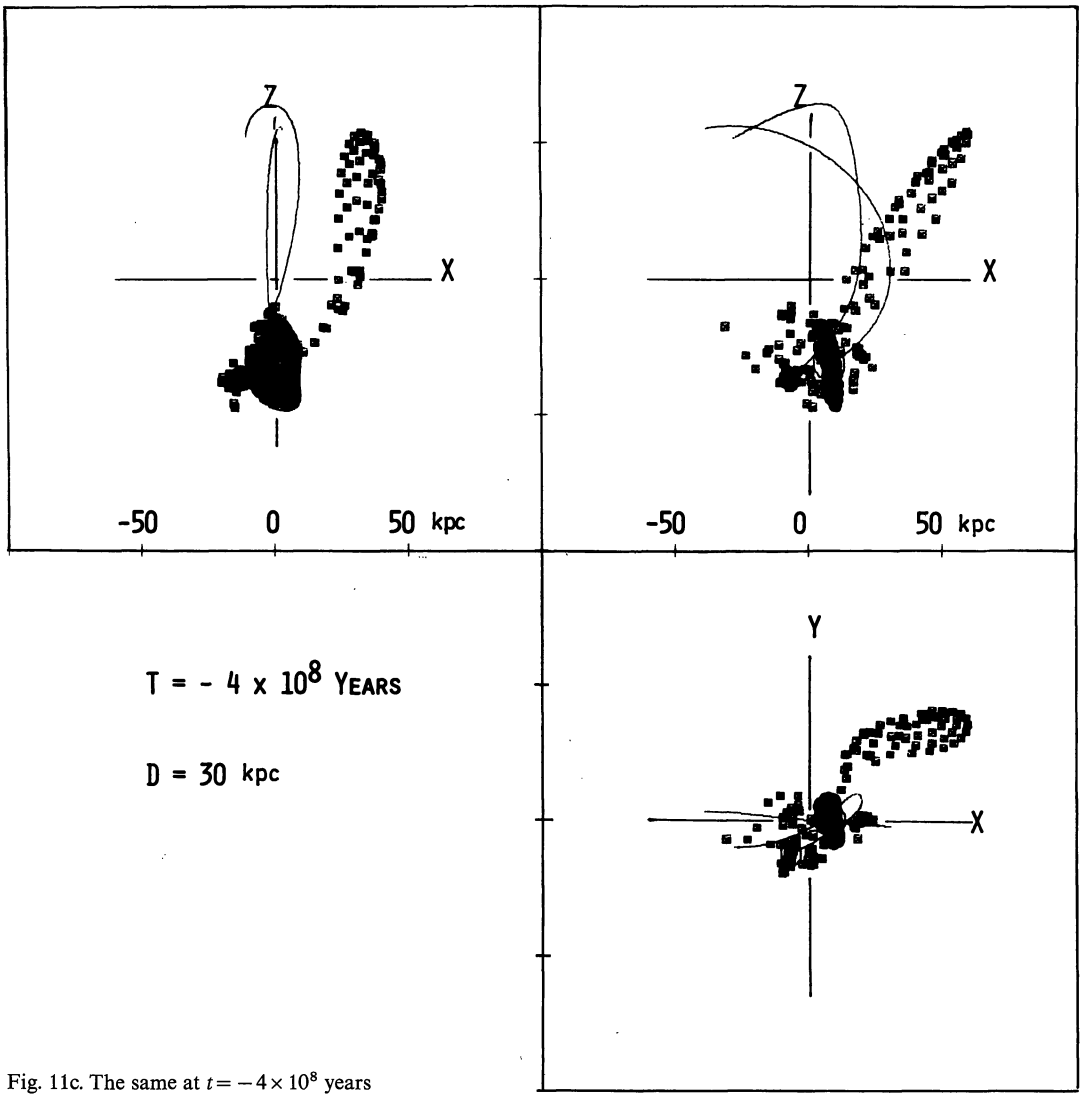

Fig. 11c. The same at $t=-4\times10^8$ years

within the corotation circle located at the galactocentric distance $R=20$ kpc. The pronounced gaseous arms observed at the rim seem, if $R=20$–25 kpc (Kerr *et al.*, 1957; Weaver, 1971; Davies, 1972), beyond the scope of this theory. If the close passage of the Magellanic Clouds to the Galaxy is correct, some of those outer arms may have been formed by tidal force instead.

Verschuur (1973) has shown that the far distant arms γ, δ and ε in his terms have large negative velocities, $v_r=-50$ to -100 km/s, in the anticenter region (see also Lindblad, 1967; Kepner, 1970; Burton and Verschuur, 1973; Heiles, 1974). Already Verschuur suggested, as a mechanism to drive such large noncircular motions, the tidal force due to the LMC: the outer arms would be pulled out during a past close passage of the LMC, and they are now falling back with the negative velocities.

We have examined this possibility on the basis of our numerical calculations for $D=20$ and 30 kpc. The systematic radial motion is, however, at most only 20–50 km/s in the anticenter region. Worse still, it is in the opposite sense to the observation [see the $(l-v_r)$ diagrams in Figs. 6 and 8]. Thus the large-scale noncircular motion with high negative velocity at $l\simeq180°$ remains open to further investigations.

In closing, we wish to stress that the present computer studies have been made only for the parameters cited in Tables 1 and 2 in the related text. As we remarked earlier, the more sensitive of those probably include the imperfectly known separation of the LMC and SMC in depth, and also our speed of galactic rotation which strongly contaminates the observed 260 and 150 km/s l.s.r. velocities of the two Clouds. It is also clear that any decrease of the mass m_L of the LMC to $10^{10}\,M_\odot$ or less would seriously modify our conclusions. The same applies even more forcibly if the total mass m_G of our Galaxy needed to be chosen (cf. Ostriker and Peebles, 1974) more than twice as large as the present value. A discussion of such effects is in preparation and will be published later.

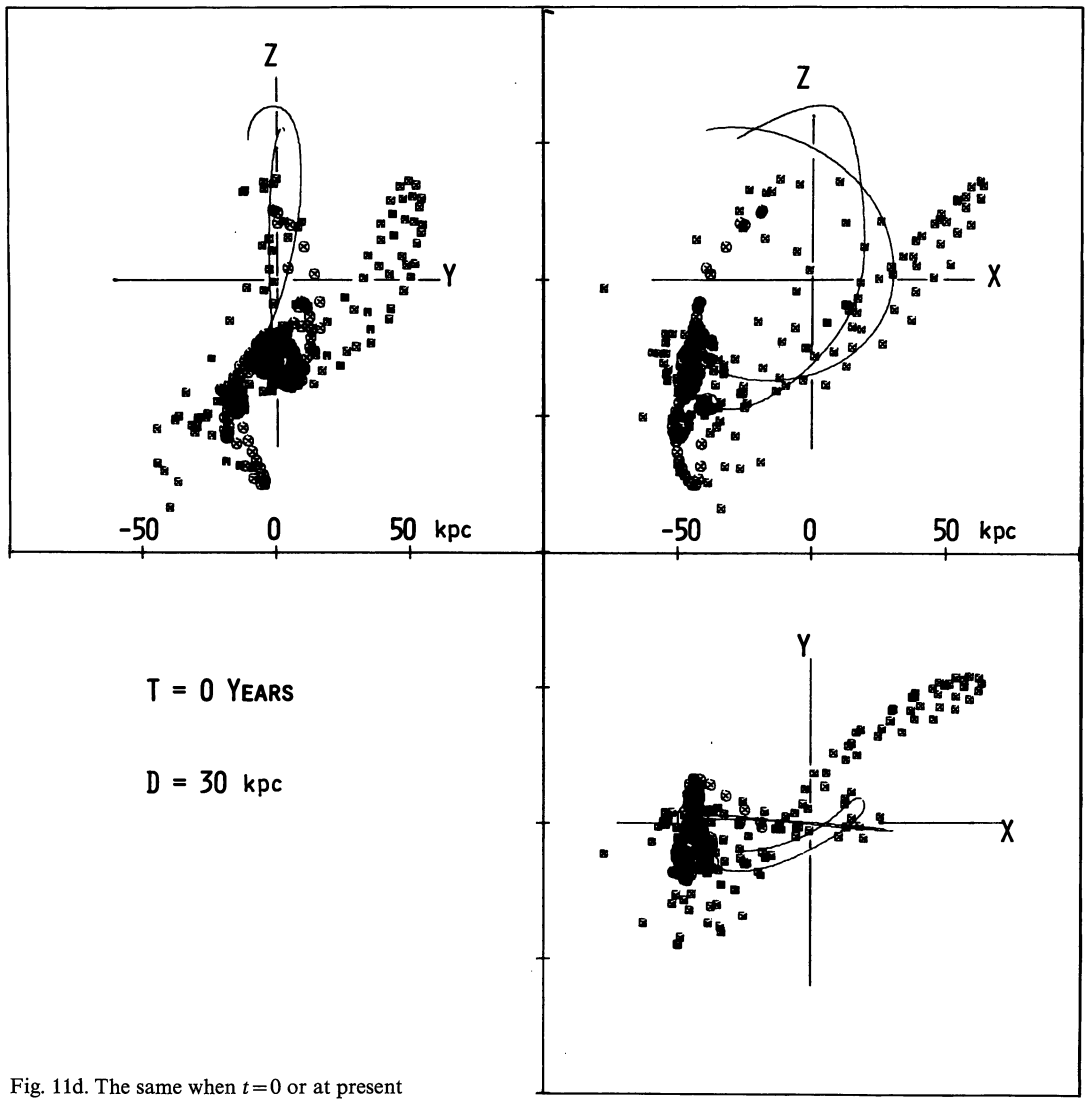

Fig. 11d. The same when $t=0$ or at present

Along the present dynamical studies among the Galaxy, LMC and SMC, some important problems arise. They will be discussed only briefly in the followings.

i) Stragglers of Test Particles

As shown in Section V, considerable portion of the test particles were pulled out of the LMC and SMC through the tidal interaction with the Galaxy, and between the Clouds themselves. Some of the pulled-out particles were shown to fall into the Galaxy, being gravitationally trapped (see Fig. 10). We may therefore expect that some objects, such as gas clouds, stars and clusters which were originally in the LMC or SMC, are now straggling in our Galaxy.

Some A-type stars are observed at $Z=1$–2 kpc with velocities exceeding 200 km/s in the Z-direction (Rodgers, 1971). Since it seems difficult to accelerate stars up to this high velocity, such extremely peculiar motions within the Galaxy could be associated with the infall of stars from the Magellanic Clouds. Note that the life-time of A-type stars is 10^9 years, being sufficiently comparable with the dynamical time-scale of the matter fall from the Magellanic Clouds.

ii) North-south Asymmetry in the Outer Rotation Curves of the Galaxy

The rotation curves of the Galaxy has been known to lack symmetry between hydrogen gases in the northern ($l=0$–$180°$) and southern ($l=180$–$360°$) sectors (see, e.g., Burton, 1973). In particular a large-scale north-south asymmetry has been observed in the cut-off velocities on the $(l-v_r)$ diagram or in the "outskirts" of the H I disk-gas as shown in Fig. 13, which implies the presence of a large-scale noncircular motion in the outermost parts of the Galaxy.

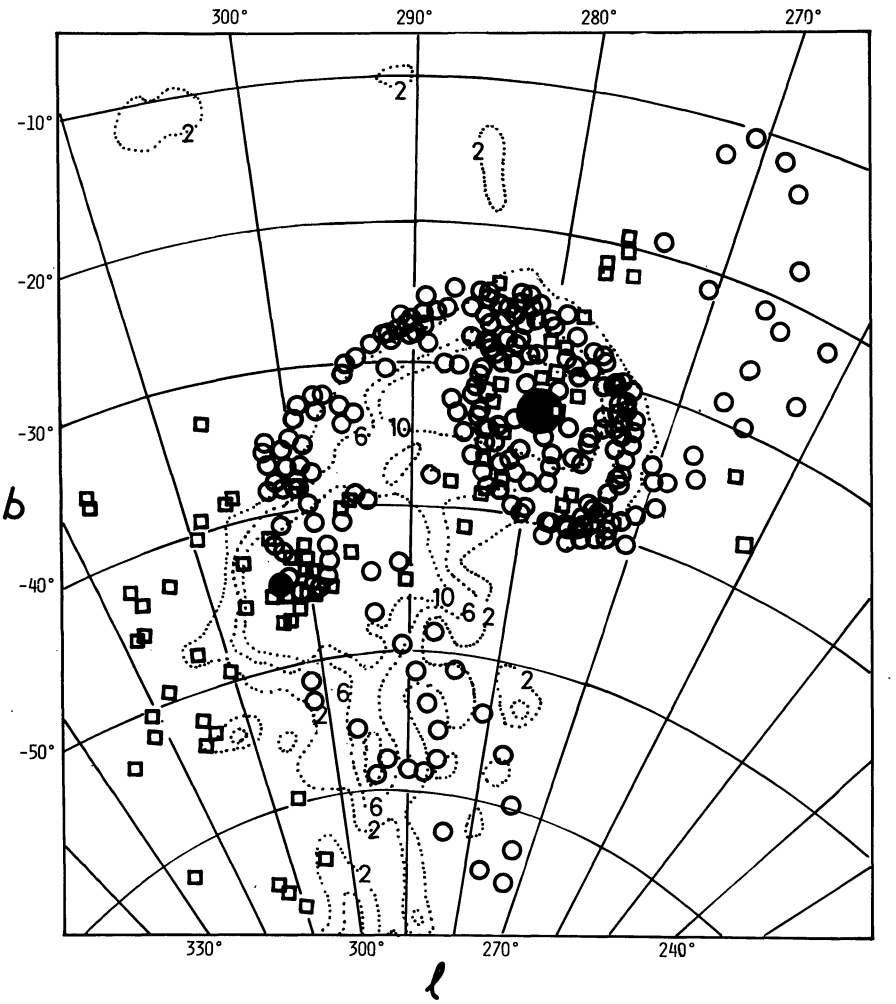

Fig. 12. Present ($t=0$) distribution of the test particles in the Magellanic Cloud region in the $D=30$ kpc orbits given in Fig. 5a as projected on the (l, b)-plane. The sky area around $(l, b)=(290°, -40°)$ in Fig. 10b is enlarged. Observed distribution of hydrogen gas is indicated by dotted contour lines, numbers on which gives the observed columnar density in units of 2×10^{9} atoms cm^{-2} (reproduced from Mathewson *et al.*, 1974). ○: particles initially in LMC, and □: initially in SMC

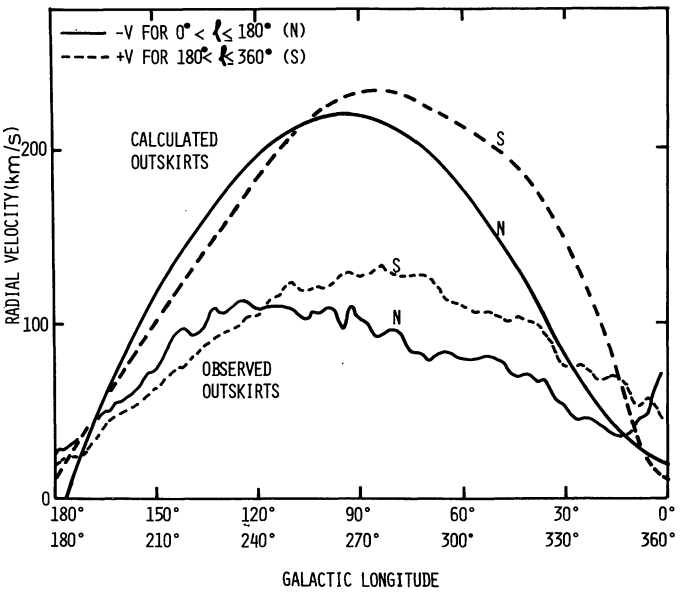

Fig. 13. North-south asymmetry in the observed cut-off velocities of H I gas (Burton, 1973) as compared with the calculated one in Fig. 8e for the outer parts of the solar circle

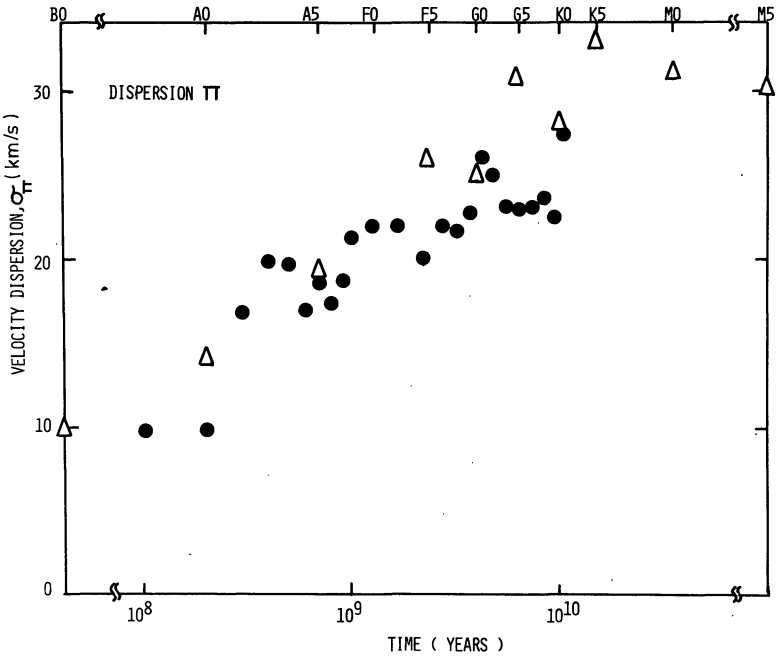

Figs. 14a—c. Computed velocity dispersions in the Y, X, and Z directions at $R \approx 10$ kpc, or σ_Π, σ_Θ and σ_Z in km/s (●). The computed dispersions are due to the tidal effect of the LMC and SMC moving along the orbits in Fig. 5a. The abscissa at the bottom indicates time reckoned from the initial epoch of the calculation. Also plotted are observed dispersions (△; Delhaye, 1965) of common stars, whose spectral types are indicated on the top of the figure

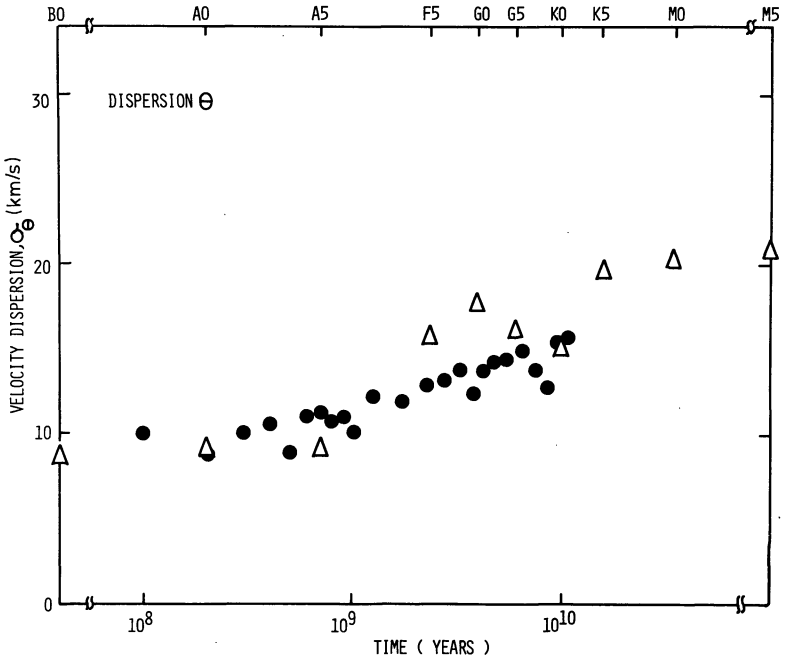

Fig. 14b

We give simultaneously in Fig. 13 the computed cut-off velocities taken from the particle motions in Fig. 8e, separately for $l = 0$–$180°$ and 180–360°. They are referred to the present solar position in the galactic circular rotation. We find a good coincidence of the computed result with the observation in phase and magnitude of the velocity differences. (The disagreement in absolute values is due mainly to detection limits of the 21-cm line observations, and also to the large disk radius adopted in the present model.) Thus, the tidal effect of the Magellanic Clouds seems a promising cause of the velocity asymmetry in the outer parts of the Galaxy.

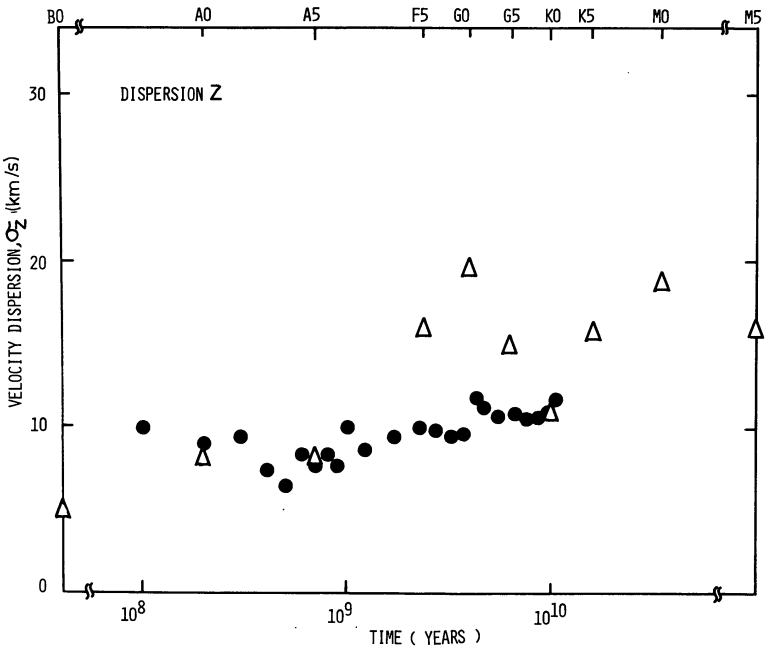

Fig. 14 c

It is difficult to know at present whether this asymmetry is connected smoothly to Kerr's (1964) asymmetry of rotation curves in the inner parts of the solar circle. Our adopted rotation curve could only roughly approximate the observation within the solar circle. However, the inner asymmetry seems due to some different mechanisms (Fujimoto, 1969; Burton, 1973; Manabe and Miyamoto, 1975), because the tidal effect decreases rapidly in general toward the center of the Galaxy and correspondingly the asymmetry should be small. Such a trend is not suggested in Kerr's asymmetry.

iii) Velocity Dispersion of the Test Particles

Random velocity of 10 km/s was initially ($t=-5\times10^9$ years) given to the test particles in circular rotation in the Galaxy. The variations of velocity dispersions in the three directions, radial σ_Π, azimuthal σ_Θ and vertical σ_Z, were computed for 10^{10} years until $t=5\times10^9$ years for the LMC's orbit of $D=30$ kpc in Fig. 5a. The result at $R\simeq10$ kpc is given by dark circles in Fig. 14, where we find that the velocity dispersions increase secularly and attain after 10^{10} years $\sigma_\Pi=25$ km/s, $\sigma_\Theta=15$ km/s and $\sigma_Z=11$ km/s.

It is observationally known that the velocity dispersions of common stars increase monotonically with the spectral type (Delhaye, 1965). Referring to the life-time of star, we have plotted the observed dispersions with open triangles in Fig. 14, in which we find a good coincidence.

Thus, the periodic close passage of the Magellanic Clouds could contribute to increasing the velocity dispersions of common stars in the Galaxy. Of course, many problems remain open to be solved, such as inward wave transport (Toomre, 1969) of the tidally induced vibrational energy of stars by the here neglected self-gravity before degrading into random motions.

The same computations were made for the $D=20$ kpc (A_4) and 40 kpc (C_4) orbits. The computed velocity dispersions were, however, twice as large as the observed ones for $D=20$ kpc, and they were too small for $D=40$ kpc, both giving no compatible results.

Acknowledgement. We wish to express our thanks to T. Omodaka and M. Fujishita for their help to our computations. We are very grateful to Professor A. Toomre for his detailed criticism and kind advice on the present work. The numerical computations were carried out on a HITAC 8500 at the Institute of Plasma Physics, Nagoya University.

References

Avner, E. S., King, I. R. 1967, *Astron. J.* **72**, 650
Burton, W. B. 1973, *Publ. Astron. Soc. Pacific*, **85**, 679
Burton, W. B., Verschuur, G. L. 1973, *Astron. & Astrophys. Suppl.* **12**, 145
Clutton-Brock, M. 1972, *Astrophys. Space Sci.* **17**, 292
Davies, R. N. 1972, *Monthly Notices Roy. Astron. Soc.* **160**, 381
Delhaye, J. 1965, in *Galactic Structure*, Ed. A. Blaauw and M. Schmidt (Univ. Chicago Press, Chicago), p. 61
de Vaucouleurs, G. 1960, *Astrophys. J.* **131**, 265
Elwert, G., Hablick, D. 1965, *Z. Astrophys.* **61**, 273
Eneev, T. M., Kozlov, N. N., Sunyaev, R. A. 1973, *Astron. & Astrophys.* **22**, 41
Fujimoto, M. 1968, *Astrophys. J.* **152**, 391
Heiles, C. 1974, *Astron. & Astrophys. Suppl.* **14**, 1
Henderson, A. P. 1966, *Latitude-Velocity Maps*, College Park, University of Maryland
Hénon, M. 1965, *Ann. Astrophys.* **28**, 992
Hindman, J. V., Kerr, F. J., McGee, R. X. 1963, *Australian J. Phys.* **16**, 570

Hindman, J. V. 1967, *Australian J. Phys.* **20**, 147
Hunter, C., Toomre, A. 1969, *Astrophys. J.* **155**, 747
Innanen, K. A. 1966, *Astrophys. J.* **143**, 153
Kepner, M. 1970, *Astron. & Astrophys.* **5**, 444
Kerr, F. J., Hindman, J. V., Carpenter, M. S. 1957, *Nature* **180**, 677
Kerr, F. J., Westerhout, G. 1965, in *Galactic Structure*, Ed. A. Blaauw and M. Schmidt (University of Chicago press), p. 167
Lin, C. C., Yuan, C., Shu, F. H. 1969, *Astrophys. J.* **155**, 721
Lindblad, P. O. 1967, *Bull. Astron. Inst. Neth.* **19**, 34
Manabe, S., Miyamoto, M. 1975, *Publ. Astron. Soc. Japan*, **27**, 35
Mathewson, D. S., Clearly, U. N., Murray, J. D. 1974, *Astrophys. J.* **190**, 291
Mathewson, D. S., Ford, V. L. 1970, *Astrophys. J.* **160**, L43
Mirabel, I. F., Turner, K. C. 1973, *Astron. & Astrophys.* **22**, 437
Ostriker, J. P., Peebles, P. J. E. 1973, *Astrophys. J.* **186**, 467
Pfleiderer, J., Siedentopf, H. 1961, *Z. Astrophys.* **51**, 201
Pfleiderer, J. 1963, *Z. Astrophys.* **58**, 12
Rodgers, A. W. 1971, *Astrophys. J.* **165**, 581
Schmidt, Th. 1970, *Astron. & Astrophys.* **6**, 294
Toomre, A. 1969, *Astrophys. J.* **158**, 899
Toomre, A. 1970, in *The Spiral Structure of our Galaxy*, IAU Symp. No. 38, Ed. B. W. Becker and G. Contopoulos, D. Reidel Publishing Co., Holland, p. 334
Toomre, A. 1972, *Quart. J. Roy. Astron. Soc.* **13**, 266
Toomre, A., Toomre, J. 1972, *Astrophys. J.* **178**, 623
Verschuur, G. L. 1973, *Astron. & Astrophys.* **22**, 139
Weaver, H. 1970, in *The Spiral Structure of our Galaxy*, IAU Symp. No. 38, Ed. B. W. Becker and G. Contopoulos, D. Reidel Publishing Co., Holland, p. 126
Wright, A. E. 1972, *Monthly Notices Roy. Astron. Soc.* **157**, 309
Yabushita, S. 1971, *Monthly Notices Roy. Astron. Soc.* **153**, 97

M. Fujimoto
Y. Sofue
Department of Physics
Nagoya University
Chikusa
Nagoya 464, Japan